



Cite this: *Ind. Chem. Mater.*, 2025, 3, 131

## Unveiling the potential of bismuth-based catalysts for electrochemical CO<sub>2</sub> reduction

Negar Sabouhanian, Jacek Lipkowski\* and Aicheng Chen \*

Electrochemical CO<sub>2</sub> reduction has favorable industrial relevance due to its integrability with renewable energies and controllable product generation. Bismuth-based catalysts have emerged as promising candidates in this regard due to their intriguing electrochemical properties and cost-effectiveness. This review focuses on recent advances in bismuth-based catalysts for the electrochemical reduction of CO<sub>2</sub>, including synthesis methods and approaches for performance improvements. Insights into product formations using Bi-based catalysts are also presented, where *in situ* FTIR and Raman spectroscopic studies are highlighted to understand the structural evolution of the catalysts and to decipher the mechanisms of CO<sub>2</sub> reduction. Further, recent progress of electrochemical CO<sub>2</sub> reduction from an industrial perspective and strategies for further development of the bismuth-based catalysts with high activity, selectivity and stability towards practical applications are discussed.

Received 3rd October 2024,  
Accepted 29th November 2024

DOI: 10.1039/d4im00126e

rsc.li/icm

Keywords: Electrochemical CO<sub>2</sub> reduction; Bismuth; Nanomaterials; Electrocatalysts; *In situ* spectroscopy.

### 1. Introduction

The incessant increase in atmospheric carbon dioxide (CO<sub>2</sub>) levels is widely recognized as the primary driver of climate

change/global warming.<sup>1,2</sup> Potential strategies for carbon capture and utilization (CCU) to mitigate CO<sub>2</sub> emissions have attracted considerable interest.<sup>3–5</sup> The electrochemical CO<sub>2</sub> reduction reaction (CO<sub>2</sub>RR) has significant potential for industrial applications as it can integrate renewable energies as power sources.<sup>6–8</sup> In this context, reports in the literature have revealed the intensive investigation of diverse electrocatalysts and CO<sub>2</sub>RR mechanisms.<sup>8–10</sup> Despite

*Electrochemical Technology Centre, Department of Chemistry, University of Guelph, 50 Stone Road East, Guelph, Ontario N1G 2W1, Canada.  
E-mail: jlipkows@uoguelph.ca, aicheng@uoguelph.ca*



**Negar Sabouhanian**

*Negar Sabouhanian is a PhD candidate at the Electrochemical Technology Centre, Department of Chemistry, University of Guelph, Canada under the co-supervision of Professor Aicheng Chen and Professor Jacek Lipkowski. She received her MSc degree in Materials Engineering, specializing in Corrosion and Protection of Materials, from the University of Tehran, Iran in 2018. Her current research focuses on developing advanced nanomaterials and electrocatalysts for clean energy technologies, particularly electrochemical reduction of carbon dioxide. With a strong passion for sustainable energy solutions, Negar is contributing to advancing green technologies through her innovative work in electrochemistry.*



**Jacek Lipkowski**

*Jacek Lipkowski is a Professor Emeritus at the University of Guelph, Ontario, Canada. He received his PhD and DSc from the University of Warsaw, Poland and moved to Canada in 1983. His research interests span several areas such as electrochemistry, surface spectroscopy and biomimetics. He has authored ~280 papers and several book chapters. Dr Lipkowski is Fellow of the Royal Society of Canada, Killam Fellow and Fellow of the International Society of Electrochemistry (ISE). He is recipient of several awards including Gold Medal, Jacques Tacussel Prize, Bioelectrochemistry Award and Frumkin Medal of ISE, Alcan Medal and John Polanyi Award of the Canadian Society for Chemistry, E. Yeager Award of ECS and Alexander von Humboldt Stiftung Research Award.*



extensive research, implementing CO<sub>2</sub> electroreduction remains constrained due to the excessive costs involved.<sup>11</sup>

Formate is one of the products of CO<sub>2</sub>RR having substantial market potential as a valuable industrial feedstock.<sup>12</sup> The formic acid/formate market is anticipated to reach one megaton per year by 2030 with various applications in medical, agriculture, and textile industries.<sup>13</sup> They are regarded as a vital intermediate for synthesizing valuable oxygen-containing compounds such as alcohols, esters, and acids in syngas catalysis. Additionally, the high density of formic acid (1.22 kg L<sup>-1</sup>) gives it a significant volumetric hydrogen capacity of 53 g H<sub>2</sub> per liter, making it a promising candidate as a liquid hydrogen carrier.<sup>14</sup> It may be utilized in energy production and storage systems such as hydrogen fuel cells.<sup>13</sup> Formate/formic acid formation by electrochemical reduction of CO<sub>2</sub> is a promising approach due to its integrability with renewable energies, relatively low cost, practical operation and being environmentally friendly.<sup>15</sup> Among various metal-based catalysts, bismuth-based materials have exhibited significant potential for the electrochemical reduction of CO<sub>2</sub> to formate with high selectivity.<sup>16</sup> Bismuth is mainly found on the ores bismuthinite (bismuth sulfide) and bismite (bismuth oxide) as well as Bi crystals with an oxide layer. Bismuth is not very reactive and can sometimes be found as a native metal.<sup>17</sup> Bi-based catalysts exhibited a lower overpotential and higher faradaic efficiency for formate formation compared with other metals. The high formate selectivity can be attributed to the low energy barrier of \*COO<sup>-</sup> intermediate formation. In addition, hydrogen evolution reaction (HER) as a competitive reaction exhibits a relatively high overpotential at Bi-based catalysts.<sup>18</sup> These factors along with the cost-effectiveness, low toxicity and high abundance in nature in

contrast to other metals make Bi-based catalysts promising for CO<sub>2</sub> reduction to formate in large-scale applications.<sup>19–24</sup> Different nanostructured monometallic Bi catalysts (*e.g.*, nanoparticles, nanorods, nanodendrites, and nanosheets) have been synthesized and investigated for CO<sub>2</sub> reduction.<sup>25</sup> However, the weaker \*OCHO binding energy makes it difficult to boost formate generation.<sup>26</sup> It has been shown that the addition of secondary elements to form bimetallic Bi-based catalysts might effectively improve their catalytic performance.<sup>27</sup> The binding energy of oxygen in \*OCHO may be adjusted by introduction of another metal (*e.g.*, CuBi,<sup>28</sup> BiSn,<sup>29</sup> InBi,<sup>30</sup> and ZnBi (ref. 31)), which may enhance the \*OCHO adsorption through compressive strain and changes of surface electronic bands structure.<sup>26</sup> Further, it is revealed that bimetallic Bi-based catalysts not only electrochemically reduce CO<sub>2</sub> to formate, but also lead to the creation of other products such as propane and ethylene.<sup>32,33</sup> *In situ* characterization techniques have been developed to study the reaction mechanisms and identify the key intermediates formed during CO<sub>2</sub> reduction. Great efforts have been made to attain industrial-compatible current densities and high stability for CO<sub>2</sub> reduction to formate on Bi-based catalysts using flow cells or membrane electrode assemblies (MEAs). However, achieving ampere level current densities and high electrode stability remains challenging.

In this review, we discuss the recent advances in the development of bismuth-based catalysts with a focus on synthesis methods and strategies for performance enhancement. The possibility of additional product generation using Bi-based catalysts reported in the recent literature is featured. The detection of key intermediates and monitoring of product formation *via in situ* FTIR and Raman spectroscopy are highlighted. Finally, recent achievements from an industrial perspective are described, and future research directions are proposed.

## 2. Monometallic Bi-based catalysts

### 2.1. Synthesis methods

Several strategies have been employed to fabricate monometallic Bi-based catalysts, including top-down exfoliation techniques, chemical reduction reactions, and the electroreduction of pre-synthesized materials (*e.g.*, BiOX where X is Cl, Br, or I,<sup>34</sup> (BiO)<sub>2</sub>CO<sub>3</sub>,<sup>35</sup> Bi<sub>2</sub>O<sub>3</sub>,<sup>21</sup> and Bi-metal organic frameworks (Bi-MOFs)).<sup>36</sup> The morphologies<sup>21</sup> and coordination environments<sup>37</sup> of Bi-containing precursors significantly affect the final structure of the Bi-based catalyst. Various surface engineering techniques have been applied to improve the faradaic efficiency (FE) of formate production, including defect engineering, heteroatom doping, and the active site reconstitution in Bi nanosheets (Bi Nss).<sup>38,39</sup> In this section, recent advances in strategies for monometallic Bi-based catalysts synthesis, and proposed strategies for enhancing their catalytic performance are reviewed.

**2.1.1. *In situ* electrochemical transformation.** Traditional strategies for the production of monometallic Bi-based



Aicheng Chen

*Aicheng Chen is a Professor of Chemistry, Director of the Electrochemical Technology Centre at the University of Guelph, and Tier 1 Canada Research Chair in Electrochemistry and Nanoscience. His research interests span the areas of electrochemistry, photoelectrochemistry, biosensors, and nanoscience. He has published ~300 journal articles. Dr Chen is Fellow of the Chemical Institute of Canada, the Royal Society of Canada, the Royal*

*Society of Chemistry (UK) and the International Society of Electrochemistry. He is recipient of the Ontario Premier's Research Excellence Award; the Lash Miller Award and the R.C. Jacobsen Award of the ECS; the Fred Beamish Award, the Keith Laidler Award, the W.A.E. McBryde Medal and the Ricardo Aroca Award of the Canadian Society for Chemistry.*



catalysts, whether through top-down or bottom-up approaches, face challenges when it comes to scaling up their production. Thus, indirect methods may offer a promising alternative for the synthesis of Bi-based catalysts,<sup>40</sup> with nanosheet morphologies getting significant attention.<sup>41</sup> Numerous unsaturated Bi atom coordination sites are available in two-dimensional (2D) Bi NSs comprised of tens of atomically thin layers, which provide ample reactive sites for CO<sub>2</sub>RR.<sup>40,42</sup> The *in situ* (electro)chemical transformation of Bi-containing pre-catalysts has gained considerable interest as an indirect method for the synthesis of Bi NS catalysts.<sup>43</sup> Changes in chemical compositions and/or structures have been widely observed during (electro)chemical transformation, giving an efficient catalyst with desirable reactive sites for CO<sub>2</sub>RR.<sup>44,45</sup> Different Bi-based pre-catalysts can endow bismuth materials with unique surface properties and local environments, strongly impacting their performance for CO<sub>2</sub> reduction.<sup>46</sup> For instance, it was demonstrated that the morphologies, particle sizes, thicknesses,<sup>40</sup> and compositions<sup>47</sup> of Bi-based precursors altered the activities of Bi-based catalysts. Wang *et al.*<sup>47</sup> prepared differently oriented bismuth oxyiodide nanosheets to adjust the ratio of basal and edge planes in derived Bi NSs. They found that during the electroreduction process, iodine and oxygen atoms were dynamically removed, leaving behind a bismuth framework. They suggested that the original bismuth oxyiodide nanosheets served as templates for catalysts of CO<sub>2</sub>RR. Their finding showed that the (004) oriented Bi<sub>5</sub>O<sub>7</sub>I NSs and (102) oriented BiOI NSs were transformed by electroreduction into basal- and edge-oriented Bi NSs, respectively. Basal-oriented Bi NSs exhibited higher selectivity for CO<sub>2</sub>RR and lower activity for HER, in contrast to edge-oriented Bi NSs. It was revealed that the

(003) basal plane played an important role in enhancing the FE due to its low activity for the competing HER. The highest FE of formate (98.0%) was achieved at -0.68 V vs. RHE for the basal-oriented Bi NSs. In another study conducted by Zheng *et al.*,<sup>43</sup> 2D bismuth oxyiodide (BiOI) was synthesized through the assembly of 1D BiOI nanotubes, which was further converted to metallic Bi *via* electroreduction. It was demonstrated that the abundant edge sites resulting from the distinct 2D Bi nanostructure ensured high selectivity for formate production. A series of BiOX nanoplates were also synthesized by Liu and coworkers<sup>40</sup> and further electroreduced by *in situ* transformations, showing that the thickness of the initial BiOX nanoplate precursor was important to maintain the 2D structure during the electroreduction. During preparation, the thickness of the BiOX nanoplates was controlled through the addition of polyvinylpyrrolidone (PVP) and mannitol. The Bi NSs derived from the electroreduction of BiOX nanoplates with an optimized thickness of ~30–40 nm exhibited a maximum FE of formate (95%) at -0.9 V vs. RHE. The thickness of Bi NSs is also an important factor, as thinner Bi NSs exhibited greater selectivity as they exposed a greater number of edge sites.<sup>36</sup> Bi NSs were synthesized from Bi<sub>2</sub>MoO<sub>6</sub> and BiOIO<sub>3</sub> precursors with two different thicknesses *via* cathodic reduction. A schematic of the preparation procedure is illustrated in Fig. 1a.<sup>36</sup> In the first stage, the Bi-containing precursors with different structures and compositions were prepared by a hydrothermal method, which then underwent long-term cathodic reduction at low potential. Interestingly, thinner Bi NSs (1.5 nm) were obtained using Bi<sub>2</sub>MoO<sub>6</sub> as an initial precursor. A corresponding SEM image of the Bi NSs produced from Bi<sub>2</sub>MoO<sub>6</sub> is presented in Fig. 1b, which shows dense arrays of large nanosheets. The electrochemical

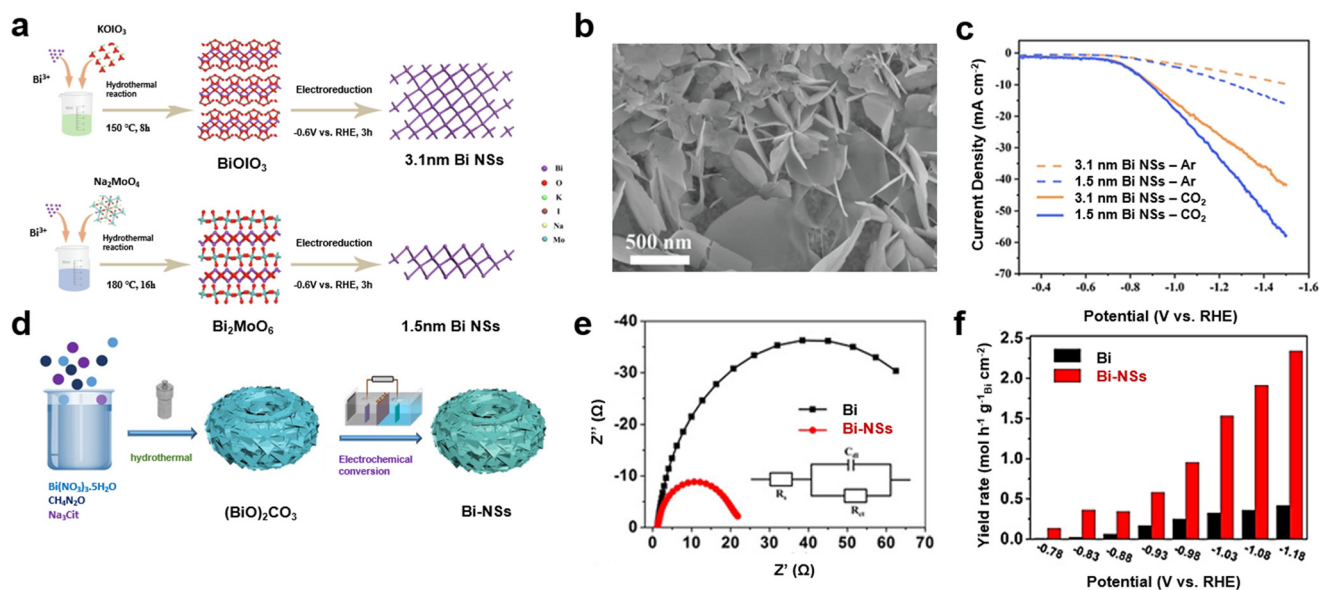


**Fig. 1** (a) Schematic of the preparation of ultrathin Bi NSs; (b) SEM image of 1.5 nm Bi NSs; (c) LSV curves for 3.1 nm Bi NSs and 1.5 nm Bi NSs in a CO<sub>2</sub> and Ar saturated 0.5 M KHCO<sub>3</sub> solution<sup>36</sup> (copyright 2023 Elsevier); (d) schematic of the preparation of Bi NSs; (e) Nyquist plots and (f) formate yielded rates for CO<sub>2</sub>RR over Bi NSs and Bi nanopowders<sup>35</sup> (copyright 2021 John Wiley and Sons).



performance of the Bi NSs was investigated with linear scanning voltammetry (LSV) in a CO<sub>2</sub> and Ar saturated 0.5 M KHCO<sub>3</sub> solution as the electrolyte. Fig. 1c depicts the LSV of the Bi NSs obtained with two different thicknesses. The thinner Bi NSs exhibited a higher current density compared to the thicker Bi NSs and showed better catalytic activity. It was revealed that thinner nanosheets generated coordination-unsaturated pits, which in turn created more edge sites leading to the higher FE of formate. Jiang *et al.*<sup>48</sup> reported on the electrochemical reconstruction of bismuth oxide formate nanowires (BiOCOOH NWs) into Bi/BiO<sub>x</sub> NSs and Bi NWs, dependent on the electrochemical reduction conditions. They demonstrated the formation of the intermediate state of Bi<sub>2</sub>O<sub>2</sub>CO<sub>3</sub> during the electroconversion of the initial precursor in a CO<sub>2</sub>-saturated KHCO<sub>3</sub> solution after 500 s, which resulted in the conversion of nanowires to 2D nanosheets. The structural evolution of the initial precursor originated from the solvent-assisted ligand exchange and further dissociation of Bi<sup>3+</sup> to form Bi<sub>2</sub>O<sub>2</sub>CO<sub>3</sub>, which served as a sacrificial template to be further electrochemically converted to Bi/BiO<sub>x</sub> NSs. This enabled easier electron transport through the 2D structure and surface oxide layer of the Bi/BiO<sub>x</sub> NSs. Their findings revealed that the presence of Bi-O structures in Bi/BiO<sub>x</sub> NSs promoted the adsorption of \*CO<sub>2</sub><sup>-</sup> and \*OCHO, which facilitated CO<sub>2</sub> activation. Similarly, the electrochemical transformation of (BiO)<sub>2</sub>CO<sub>3</sub> to Bi NSs was reported by Peng *et al.*<sup>35</sup> A schematic of the preparation of Bi NSs is presented in Fig. 1d. The initial (BiO)<sub>2</sub>CO<sub>3</sub> precursor with a persimmon-like morphology was synthesized by a hydrothermal method, which served as a self-template to be electrochemically converted to Bi NSs. The electron transfer capacity was evaluated by the electrochemical impedance spectroscopy (EIS) as shown in Fig. 1e. The smaller charge transfer resistance of Bi NSs was due to the reduced distance for electron transport in the integrative intercrossed network structure. Fig. 1f reveals that the formate yield rate was significantly higher for Bi NSs compared with commercial Bi nanopowders, due to more exposed active sites.

**2.1.2. Metal-organic framework (MOF).** Metal-organic frameworks (MOFs) represent a class of materials comprising an organized and extended structure of metal ions linked together by rigid organic ligands.<sup>49,50</sup> The organic linkers in the MOF structure can alter the adsorption behavior of water and CO<sub>2</sub> reduction intermediates, to improve the selectivity of CO<sub>2</sub>RR.<sup>51</sup> Further, the permanent porosity of MOFs makes them interesting materials for an extensive range of applications. Covalent organic frameworks (COFs) may act as electron current collectors and enhance the adsorption of intermediates.<sup>52</sup> Electrochemical CO<sub>2</sub> reduction has been reported in recent publications using Bi-containing MOFs.<sup>53</sup> Bi-MOFs were utilized directly as catalysts or indirectly as pre-catalysts for further reconstruction to form highly active and selective Bi-based materials for CO<sub>2</sub>RR. For example, a cost-effective TAL-33 MOF material was synthesized followed

by optimized carbonization and used directly as a catalyst with metallic Bi sites for the conversion of CO<sub>2</sub>RR to formate, with the FE attaining 100%.<sup>13</sup> Bi-BTC MOF (CAU-17) was prepared and investigated for CO<sub>2</sub>RR in another study, which exhibited a 92.2% FE of formate at -0.9 V vs. RHE, with over 30 h of stability. In contrast to other Bi-based catalysts (*e.g.*, Bi NSs) that were rapidly and completely reduced from Bi(+3) to metallic Bi(0), it was suggested that the MOF structure could preserve Bi in the +3 oxidation state during CO<sub>2</sub>RR based on the *in situ* X-ray absorption near-edge structure (XANES) spectroscopic measurements.<sup>51</sup> In another study by Liu *et al.*,<sup>54</sup> the Bi-MOF was coated on a gas diffusion electrode and used as a catalyst for CO<sub>2</sub>RR. A solvothermal method was employed to prepare the Bi-MOF using Bi(NO<sub>3</sub>)<sub>3</sub>·5H<sub>2</sub>O and H<sub>3</sub>BTC, which were added into methanol and dimethylformamide (DMF) solutions. Following CO<sub>2</sub>RR, surface reconstruction was observed where the initially smooth surface was converted to perpendicular sheets with nanoscale flakes on the surface. A study of the phase evolution revealed that the Bi-MOF was partially reduced to metallic Bi and partially converted to the Bi<sub>2</sub>O<sub>2.5</sub> phase. It was proposed that the Bi/Bi-O interface facilitated the adsorption of intermediates, which resulted in improving CO<sub>2</sub>RR activities and HCOOH selectivity. Recent studies have reported that Bi-O bonds can facilitate CO<sub>2</sub> adsorption and \*OOCH intermediate formation; thus, enhancing the FE of formate. Consequently, Bi-based catalysts containing Bi-O bonds such as bismuth oxides (Bi<sub>2</sub>O<sub>3</sub>) and Bi<sub>2</sub>O<sub>2</sub>CO<sub>3</sub> have been synthesized and evaluated for CO<sub>2</sub>RR.<sup>25</sup> It was reported that some Bi-MOFs were *in situ* reconstructed to Bi<sub>2</sub>O<sub>2</sub>CO<sub>3</sub>, which is the active material for CO<sub>2</sub>RR.<sup>55</sup> Cao *et al.*<sup>56</sup> synthesized a Bi-based MOF material Bi<sub>2</sub>(BDC)<sub>3</sub> (referred to as Bi-BDC) *via* a solvothermal method at an optimized temperature (120 °C) to create sphere-like structures assembled by small nanowires. It exhibited a higher current density compared to commercial Bi<sub>2</sub>O<sub>3</sub> catalysts, indicating superior catalytic activities. The structural evolution during the CO<sub>2</sub>RR was investigated and it was found that the catalyst was transformed into a pore-rich volcanic stone-like morphology after electrolysis. Their results confirmed that the Bi-BDC MOF catalyst was converted to Bi<sub>2</sub>O<sub>2</sub>CO<sub>3</sub>. The Bi-O bonds of Bi-carboxylate MOF can be destroyed by bicarbonate ions in solution, leading to its *in situ* reconstruction to Bi<sub>2</sub>O<sub>2</sub>CO<sub>3</sub>. The formate FE was ~90% after 36 h of CO<sub>2</sub>RR, showing long-term stability for formate generation, because Bi<sub>2</sub>O<sub>2</sub>CO<sub>3</sub> could maintain active Bi-O sites in the structure. Based on density-functional theory (DFT) calculations, it was revealed that the initial hydrogenation step was the rate-determining step, and the CO<sub>2</sub> reduction on the Bi-BDC catalyst occurred through proton-coupled electron transfer (PCET) *via* the \*OCHO intermediate, leading to the high selectivity of formate generation. Huang *et al.*<sup>57</sup> also reported the reconstruction of Bi-MOF (Bi-BTC) to Bi<sub>2</sub>O<sub>2</sub>CO<sub>3</sub>. The XRD results shown in Fig. 2a confirmed the formation of Bi<sub>2</sub>O<sub>2</sub>CO<sub>3</sub> after 5 min of electrolysis. The assigned peaks of Bi<sub>2</sub>O<sub>2</sub>CO<sub>3</sub> gradually



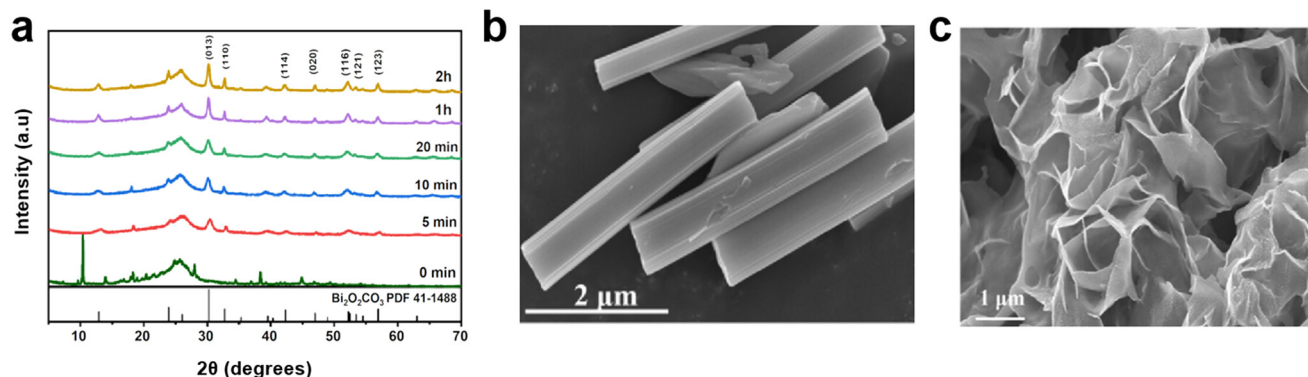


**Fig. 2** (a) XRD patterns of Bi-BTC after different electrolysis times (0 min, 5 min, 10 min, 20 min, 1 h, and 2 h); SEM image of Bi-BTC (b) before and (c) following electrolysis<sup>57</sup> (copyright 2024 American Chemical Society).

sharpened through prolonged electrolysis, due to the creation of  $\text{Bi}_2\text{O}_2\text{CO}_3$  with a well-defined crystal shape. The SEM images of the Bi-BTC MOF before and following electrolysis are presented in Fig. 2b and c. The transformation of the Bi-MOF with a nanocolumn morphology to Bi NSs possessing an ultrathin nanosheet structure after electrolysis could be clearly observed. This morphological transition was due to the charge attraction between hard base ions ( $\text{HCO}_3^-$ ) and the intermediate acid ( $\text{Bi}^{3+}$ ) that could destroy Bi–O bonds in the Bi-MOF.

**2.1.3. Other methods.** Solution-based synthesis strategies including solvothermal or chemical reduction have been proposed for the preparation of Bi-based catalysts.  $\text{NaBH}_4$  has been used as a reductant to chemically reduce  $\text{Bi}(\text{NO}_3)_3$  (ref. 38) or  $\text{BiCl}_3$  (ref. 58) as Bi precursors, to synthesize Bi NSs with an FE of formate of >90%. It was shown that the reducing capacity of the solvents and reductants could alter the morphology of the synthesized Bi nanomaterials. For example, Yu *et al.*<sup>59</sup> controlled the reduction rate of  $\text{Bi}(\text{NO}_3)_3 \cdot 5\text{H}_2\text{O}$ , and realized that the slow reduction rate facilitated by the solvothermal method resulted in the formation of porous Bi NSs. However, a fast reduction rate through the addition of  $\text{NaBH}_4$  resulted in the formation of Bi nanoparticles. The feasibility and scalability of wet chemical methods made them interesting for the synthesis of Bi-based catalysts.

## 2.2. Strategies for improving performance

Defect engineering has been employed as an effective strategy to enhance  $\text{CO}_2\text{RR}$  performance by improving selectivity, activity and stability of the catalyst. The grain boundaries in polycrystalline materials may create sites with improved activity for  $\text{CO}_2$  reduction in comparison to the competing HER.<sup>60</sup> The selectivity of Bi-based catalysts is enhanced by improving the affinity to the \*OCHO intermediate. It has been shown that the adequate exposure of edge sites and defects is a successful approach for improving the selectivity of the Bi-based catalysts in  $\text{CO}_2\text{RR}$ .<sup>16,34,36</sup> The defects of reconstructed Bi strongly depend on the initial morphology

and coordination environment of Bi-based pre-catalysts.<sup>37</sup> For example, bismuth oxide nanosheets could be converted into porous bismuth nanosheets (Bi PNSs) with abundant kink sites on the pore walls,<sup>61</sup> or converted to Bi nanoribbons by an in-plane confined hydrogen-reduction strategy with abundant Bi–O edge sites.<sup>62</sup> Bismuth sulfide ( $\text{Bi}_2\text{S}_3$ ) nanorods were electroreduced to defect-rich metallic Bi.<sup>63</sup> The major impacts of the preferential exposure sites and defect engineering were studied by Xu and coworkers.<sup>34</sup> The authors synthesized BiOBr nanosheets as Bi-containing precursors using a hydrothermal method, which was then converted to Bi NSs by topotactic transformation. As distinct Bi sources, cetyltrimethylammonium bromide (CTAB) and KBr were used during the hydrothermal process to control crystallization and form BiOBr NS with rich edge and terrace sites, respectively. Following topotactic transformation, preferential exposure sites were maintained, and a certain quantity of defect sites was also produced. DFT calculations were performed to evaluate the effects of edge sites, terrace sites, and defects on \*OCHO intermediate formation as the most energetically favored reaction pathway toward formate creation. It was revealed that the formation energy of \*OCHO on the Bi-edge sites was lower than that of the terrace sites, and defects on the edge sites could further decrease its Gibbs-free energy. It was determined that the edge/defect-rich Bi NS with a dramatically enlarged surface area exhibited high performance for  $\text{CO}_2\text{RR}$  with a current density of up to  $870 \text{ mA cm}^{-2}$  at  $-1.08 \text{ V vs. RHE}$  and FE higher than 90% for formate generation. In another study conducted by Wang *et al.*,<sup>64</sup> metal Bi with abundant defects (Bi-D) was synthesized *via* a solvothermal method and showed a 93.9% FE of formate at  $-0.9 \text{ V vs. RHE}$ . The presence of amorphous phases introduced abundant defects and unsaturated active sites that could enhance the FE compared with commercial Bi powder. The introduction of oxygen vacancies as defects was shown by Ren *et al.*<sup>65</sup> to increase the activity and selectivity in a wide potential window, where the 2D Bi/ $\text{Bi}_2\text{O}_3$  catalyst that possessed abundant oxygen vacancies ( $\text{Bi}/\text{Bi}_2\text{O}_3\text{-O}_v$ ) exhibited high selectivity for the generation of formate with an FE of >90% in a wide potential range of  $-0.7$  to



-1.35 V (RHE). It was shown that the modified adsorbing-desorbing property was due to the abundant oxygen vacancies provided adsorption sites for CO<sub>2</sub> molecules on the catalyst surface. CO<sub>2</sub> molecules were thus ready to be reduced even at high negative potentials (up to -1.35 V (RHE)). The FE of formate remained at around 90% with no obvious decrease after 200 h at -0.8 and -0.85 V (RHE), showing the high stability of Bi/Bi<sub>2</sub>O<sub>3</sub>-O<sub>v</sub> catalyst. In addition to oxygen vacancies, amorphous regions as indicated in Fig. 3a (red dotted circles) were observed. The Bi/Bi<sub>2</sub>O<sub>3</sub>-O<sub>v</sub> catalyst showed a higher formate FE than the same catalysts without oxygen vacancies (Fig. 3b). DFT calculations revealed that the Bi/Bi<sub>2</sub>O<sub>3</sub>-O<sub>v</sub> catalyst exhibited a lower energy barrier for \*OCHO formation than the Bi/Bi<sub>2</sub>O<sub>3</sub> catalyst (Fig. 3c), confirming the higher activity and selectivity of Bi/Bi<sub>2</sub>O<sub>3</sub>-O<sub>v</sub> for CO<sub>2</sub>RR to formate in a wide range of potential. The numerous O vacancies were suggested to create frustrated Lewis pairs (FLPs) on the surface to promote CO<sub>2</sub>RR.

The creation of disordered metal sites has been proposed by Wang *et al.*<sup>19</sup> as an efficient defect engineering strategy to activate CO<sub>2</sub> and enhance activity for formate formation. It has been suggested that CO<sub>2</sub> molecules tended to be adsorbed to and activated on the disorder-engineered Bi sites. It was observed that the distorted metal sites could enhance localized electron transfer to the antibonding π\* orbital of adsorbed CO<sub>2</sub> to bend the linear CO<sub>2</sub> molecules. The richly lattice distorted Bi NSs exhibited a high value of formate FE, reaching ~100% at a current density of 200 mA cm<sup>-2</sup>.

It was confirmed that the introduction of p-block atoms into bismuth could modify its electronic structure and alter

the energy required for the generation of intermediates.<sup>67</sup> The introduction of appropriate heteroatoms may modify the electronic density of Bi p-orbitals, thus enhancing the adsorption of the \*OCHO intermediates and improving the intrinsic activity for CO<sub>2</sub> reduction.<sup>68</sup> For instance, the edge defects of Bi NSs may be coordinated by heteroatom dopants such as sulfur,<sup>37,66</sup> titanium,<sup>69</sup> or copper<sup>39</sup> to enhance CO<sub>2</sub>RR selectivity, while suppressing the competing HER. Chen *et al.*<sup>67</sup> showed that boron doping could induce the formation of electron-rich Bi, thus facilitating the reduction of \*OCHO. A similar electron enrichment effect was also observed by Ti doping, which enhanced interactions between the active sites and \*OCHO intermediates. For pure Bi, \*OCHO intermediates are strongly adsorbed on the surface, making them difficult to desorb as formate.<sup>67</sup> It was revealed that the electron enrichment of Bi could weaken the binding strengths between the active metal centers and oxygen atoms, thereby lowering the barrier for generating \*OCHO intermediate.<sup>69</sup> Furthermore, the formation of H\* as a key intermediate for HER may be strongly suppressed by doping.<sup>67</sup> A recent study conducted by Wang *et al.*<sup>66</sup> demonstrated that sulfur doping not only induced charge redistribution around Bi atoms but also activated water molecules to provide sufficient H<sub>ad</sub>\* for CO<sub>2</sub>RR rather than HER (Fig. 3d) to optimize the reaction pathway toward formate formation. The HR-STEM image of S-doped Bi in Fig. 3e revealed a profusion of defects due to the breaking of Bi-O bonds in the initial Bi-containing precursor following topotactic transformation. The effects of sulfur doping on the catalytic activity of Bi NSs were investigated using DFT

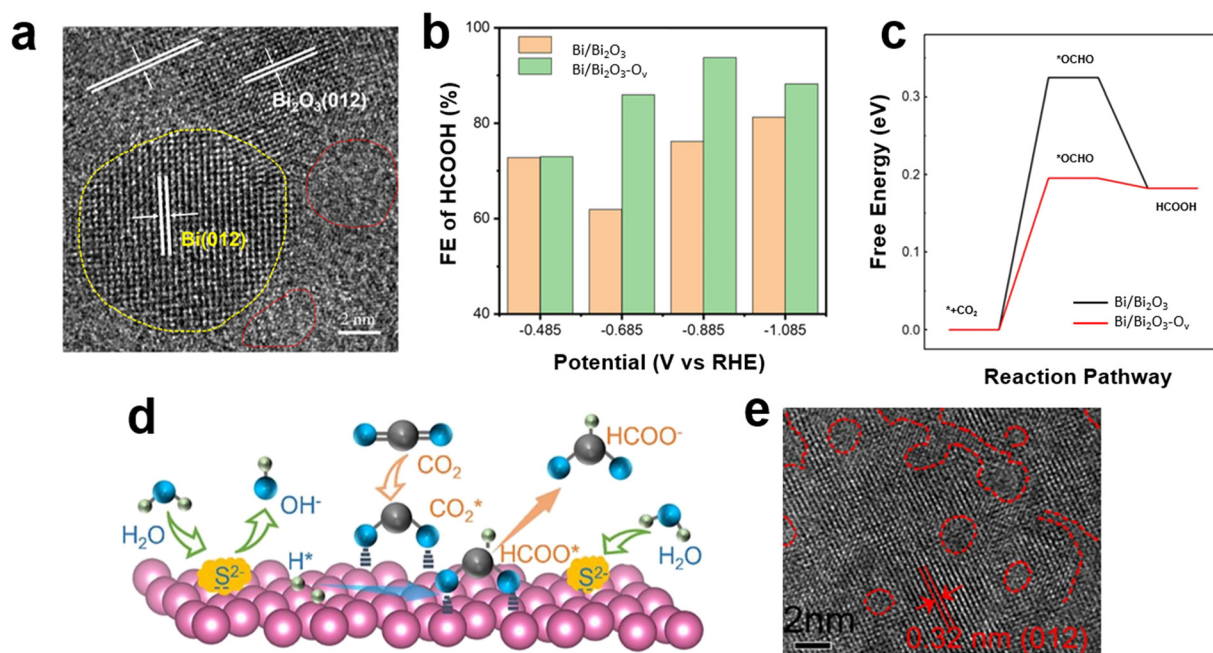


**Fig. 3** (a) HRTEM image of Bi/Bi<sub>2</sub>O<sub>3</sub>-O<sub>v</sub>; (b) FE of formate for Bi/Bi<sub>2</sub>O<sub>3</sub> and Bi/Bi<sub>2</sub>O<sub>3</sub>-O<sub>v</sub> catalysts measured at different potentials in flow cells using 1 M KOH electrolyte; (c) free energy diagrams of CO<sub>2</sub>RR to formate using Bi/Bi<sub>2</sub>O<sub>3</sub> and Bi/Bi<sub>2</sub>O<sub>3</sub>-O<sub>v</sub> catalysts<sup>65</sup> (copyright 2022 John Wiley and Sons); (d) schematic of CO<sub>2</sub> reduction mechanism using Bi-S<sub>2</sub> catalyst; (e) HR-TEM image for Bi-S<sub>2</sub> catalysts<sup>66</sup> (copyright 2023 Elsevier).



calculations as reported by Lv *et al.*,<sup>37</sup> indicating that sulfur dopants existed primarily at the edge sites of Bi NSs. This translated to the strong adsorption capacities of \*OCHO intermediates while inhibiting the production of CO and H<sub>2</sub>.

Recent studies have claimed that the bismuth subcarbonate (Bi<sub>2</sub>O<sub>2</sub>CO<sub>3</sub>) is a stable Bi phase under CO<sub>2</sub>RR that may serve as the active phase for the generation of formate.<sup>70</sup> Bi<sub>2</sub>O<sub>2</sub>CO<sub>3</sub> can provide high carrier mobility due to its thin thickness and limits nanoparticle growth, preventing disordered aggregation and preserving the number of active sites.<sup>26</sup> The establishment of the Bi–Bi<sub>2</sub>O<sub>2</sub>CO<sub>3</sub> interface has been suggested as an efficient strategy to promote CO<sub>2</sub> activation and the formation of key intermediates.<sup>63</sup> Liu *et al.*<sup>25</sup> synthesized flower-like Bi NSs and confirmed the formation of stable Bi–Bi<sub>2</sub>O<sub>2</sub>CO<sub>3</sub> interfaces after exposure to air. It was shown that the electrode containing Bi–Bi<sub>2</sub>O<sub>2</sub>CO<sub>3</sub> interfaces exhibited improved CO<sub>2</sub> reduction activity in contrast to the bulk Bi electrode, and the FE of formate could be enhanced up to 89% at –1.07 V vs. RHE. Two-dimensional nanoflake Bi<sub>2</sub>O<sub>2</sub>CO<sub>3</sub> was utilized as a substrate to load InO<sub>x</sub> nanodots for efficient CO<sub>2</sub> reduction to formate. A good performance of the catalysts with a high FE of 90.83% at a current density of 200 mA cm<sup>–2</sup> was attributed to the exposure of the active sites.<sup>26</sup>

### 3. Bimetallic Bi-based catalysts

Bimetallic electrocatalysts typically exhibit higher activity and selectivity for CO<sub>2</sub> reduction in contrast to monometallic catalysts since it is an effective approach for adjusting the composition, stabilizing key intermediates, optimizing the

electronic structure, and suppressing competing reactions.<sup>20,71,72</sup> The careful and rational design of the alloy composition and structure can enhance the selective adsorption of intermediates at active sites, lowering activation barriers and favoring desired reaction pathways. In this section, recently reported Bi-based bimetallic catalysts for the generation of formate and other products are reviewed.

#### 3.1. Formate generation

Cu and Bi have been widely investigated in bimetallic systems to augment the generation of formate.<sup>73</sup> The introduction of Cu into Bi enables the reduction of the energy barriers for intermediate formation through effective electronic structure modifications, facilitating the creation of formate.<sup>74,75</sup> Yang *et al.*<sup>76</sup> studied the effect of electronic structure modifications on the CO<sub>2</sub> adsorption at Bi, Bi/Cu<sub>9</sub>S<sub>5</sub>, and Bi/Cu<sub>9</sub>S<sub>8</sub> catalysts. The projected density of states (PDOS) results showed that the interaction of \*OCHO with Bi was mainly due to the s-p orbital hybridization. However, the heterojunctions Bi/Cu<sub>9</sub>S<sub>5</sub> and Bi/Cu<sub>9</sub>S<sub>8</sub> provided more Bi orbital hybridization mainly due to the p-d orbital hybridization, enhancing the adsorption of \*OCHO intermediate. Recently, differently structured CuBi catalysts were synthesized utilizing various techniques (*e.g.*, electrodeposition,<sup>72</sup> hydrothermal,<sup>77</sup> derivations from MOFs,<sup>78</sup> and galvanic exchange reactions<sup>11</sup>). Liu *et al.*<sup>79</sup> synthesized BiCu on a Cu foam by coupling a hydrothermal reaction followed by electrochemical transformation. Cu<sup>2+</sup> and Bi<sup>3+</sup> ions were co-deposited on a Cu foam to create a

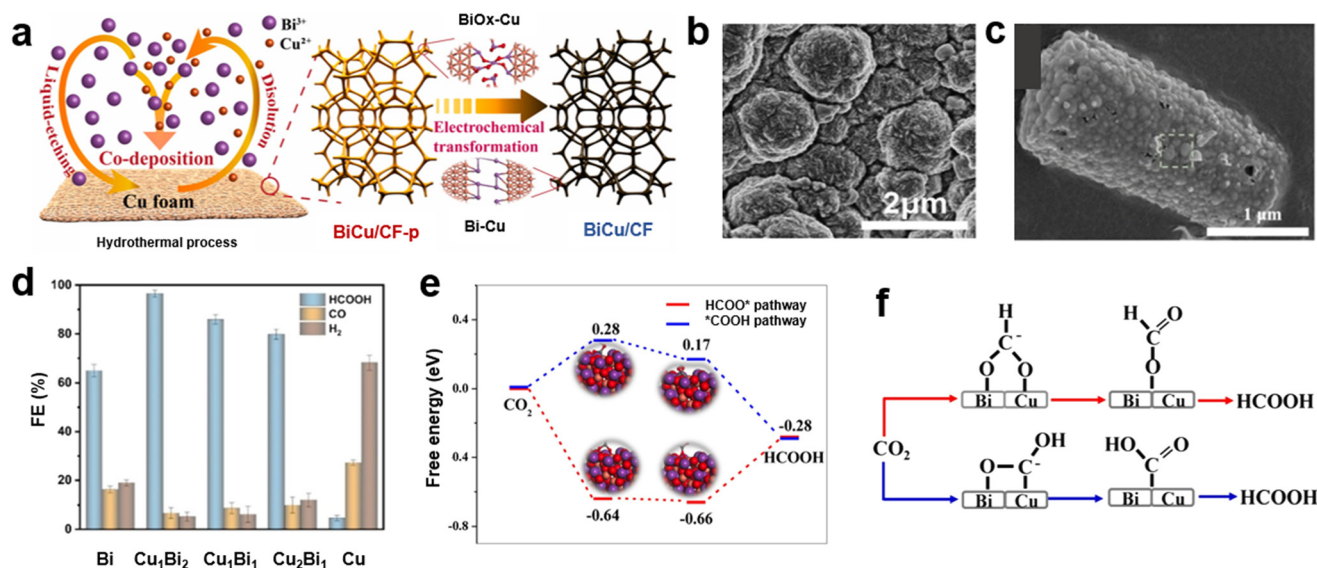


**Fig. 4** (a) Schematic of fabrication pathway for a BiCu/CF electrode<sup>79</sup> (copyright 2022 Elsevier); (b) SEM image of CuBi bimetallic catalyst electrode synthesized at –0.6 V<sup>73</sup> (copyright 2022 Elsevier); (c) SEM image of the optimized Cu<sub>1</sub>–Bi/Bi<sub>2</sub>O<sub>3</sub>@C catalyst<sup>78</sup> (copyright 2022 John Wiley and Sons); (d) FE of CO<sub>2</sub>RR over Cu–Bi electrocatalysts at –0.9 V (vs. RHE)<sup>81</sup> (copyright 2022 John Wiley and Sons); (e) free energy diagrams of various pathways of CO<sub>2</sub>RR to formate on a CuBi75 (211) plane and (f) proposed mechanism of CO<sub>2</sub> reduction on the CuBi75 catalyst<sup>82</sup> (copyright 2021 Elsevier).



BiCu pre-catalyst (BiCu/CF-p), which had close interactions between Bi and Cu. After further electrochemical transformation, the obtained bimetallic BiCu catalyst on Cu foam (BiCu/CF) exhibited an unexpectedly high formate current density. Fig. 4a illustrates their synthesis procedures, which show that the delocalization of Bi p-orbitals induced by nearby metal Cu atoms enhanced the CO<sub>2</sub>RR pathway. This interaction facilitated the hybridization of orbitals of Bi atoms and \*OCHO intermediates, which created additional anti-bonding orbitals. Consequently, the \*OCHO intermediates were stabilized and the thermodynamic barrier of CO<sub>2</sub>RR was reduced. Similarly, Lou *et al.*<sup>73</sup> successfully co-electrodeposited CuBi bimetallic catalysts on a derived copper foam using complexing agents like trisodium citrate dehydrate in the electrolyte solution. In this work, the researchers confirmed that the applied potential for co-electrodeposition had a significant impact on the growth mode of the catalyst, which altered its performance to selectively convert CO<sub>2</sub> to formate. It was observed that a needle-like bimetallic CuBi structure (Fig. 4b) was formed at -0.6 V (Ag/AgCl), which had irregular coverage and showed the highest formate FE (94.4%) at -0.97 V (RHE). The tip of the needles could enhance the concentration of the adsorbed

CO<sub>2</sub> on the catalyst surface due to the field-induced reagent concentration (FIRC) effect. In another study conducted by Xue *et al.*<sup>78</sup> a novel Cu/Bi bimetallic catalyst with a cylindrical morphology containing bimetallic nanoparticles was derived from MOFs (Fig. 4c). The FE of formate attained 93% at -0.94 V (RHE), which was attributed to the stronger adsorption of CO<sub>2</sub><sup>-</sup> intermediates. The electron transfer of Cu to Bi could tune the binding strength of CO<sub>2</sub><sup>-</sup> intermediates, leading to improving electrocatalytic selectivity toward formate. A new strategy for the synthesis of 3D Cu–Bi nanofoam electrodes was reported by Yang *et al.*,<sup>80</sup> who employed a rapid thermal shock synthesis technique followed by porosity engineering *via* acid etching and electroreduction.

In addition to the morphologies of the bimetallic CuBi catalysts, their compositions played key roles in determining their activities<sup>77</sup> and selectivities.<sup>32</sup> Li *et al.*<sup>81</sup> prepared self-supporting Cu–Bi aerogel catalysts at different molar ratios (Fig. 4d) and showed that the selectivity could be modified by altering the molar ratio of Cu/Bi. A high formate FE (96.57%) was achieved using a Cu<sub>1</sub>Bi<sub>2</sub> catalyst. They suggested that the 3D self-supporting structure and high surface area of Cu–Bi aerogels could facilitate electron transfer through more transport channels. As a result, it enhanced the reaction of

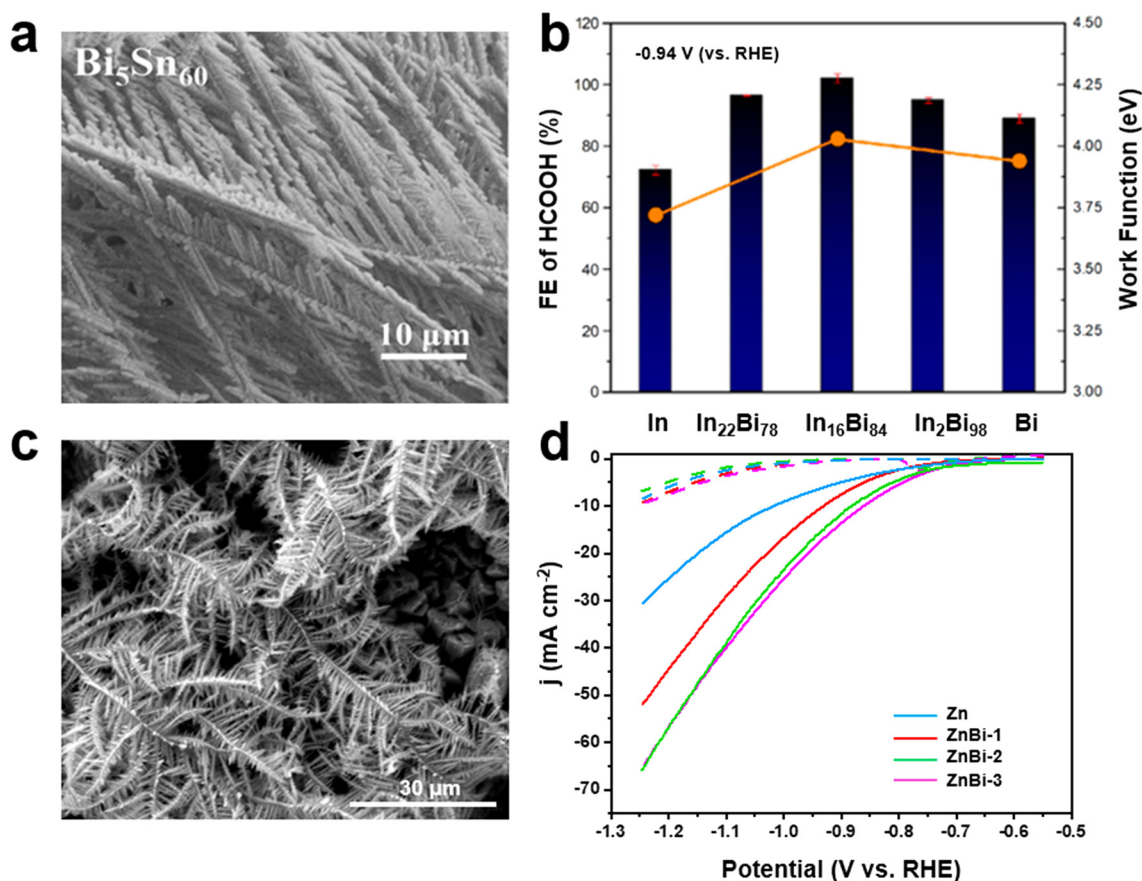


Fig. 5 (a) SEM image of Bi<sub>5</sub>Sn<sub>60</sub> catalyst<sup>29</sup> (copyright 2022 Elsevier); (b) the measured FE of formate for InBi catalysts with different compositions at -0.94 V (solid bar) and the DFT-calculated WF for In, In<sub>16</sub>Bi<sub>84</sub>, and Bi (orange line)<sup>30</sup> (copyright 2022 American Chemical Society); (c) SEM image of the ZnBi-3 electrode at 3000× magnification. (d) LSV curves of Zn and ZnBi electrodes recorded at a 20 mV s<sup>-1</sup> scan rate for CO<sub>2</sub>RR (solid lines) and HER (dashed lines)<sup>86</sup> (copyright 2024 American Chemical Society).



the intermediates with protons/electrons, leading to higher CO<sub>2</sub>RR catalytic efficiency. In another study, a composite Cu<sub>1</sub>-Bi<sub>1</sub> bimetallic catalyst with a ginger root-like structure (CuO/CuBi<sub>2</sub>O<sub>4</sub>) was synthesized by Ren *et al.*,<sup>83</sup> which exhibited a high FE (98.07%) for formate at -0.98 V *vs.* RHE. It was demonstrated that the Cu-Bi interface could provide abundant active sites for CO<sub>2</sub>RR, and the presence of bismuth-oxygen bonds stabilized the adsorbed CO<sub>2</sub><sup>\*</sup> intermediate. According to the literature, it was demonstrated that the conversion of CO<sub>2</sub> to formate on CuBi catalysts was more favorable through the HCOO\* pathway since it was considerably downhill in energy (-0.66 eV). The corresponding free energy diagram of different pathways and the proposed mechanism of CO<sub>2</sub> reduction are shown in Fig. 4e and f.<sup>82</sup> CO<sub>2</sub> was preferably converted to formate with the HCOO\* intermediate.

Recently, bimetallic bismuth-based catalysts integrated with other metals such as Sn, In, and Zn have been explored. For instance, bimetallic Bi/Sn catalysts were prepared by a two-step electrodeposition method,<sup>29</sup> and it was found that the morphology and catalytic activity could be greatly affected by the deposition time. The needle-like structure in Fig. 5a was created through the deposition of metallic Bi for 5 min followed by the deposition of metallic Sn for 60 min (Bi<sub>5</sub>Sn<sub>60</sub>) on a copper mesh substrate. It was demonstrated that Bi<sub>5</sub>Sn<sub>60</sub> had a high formate production rate (634.3 μmol cm<sup>-2</sup> h<sup>-1</sup>) at -1.0 V (*vs.* RHE). This remarkable formate generation rate was related to the modification of the electronic structure, which enhanced the interactions between the active sites and \*OCHO intermediates. A facile co-electrodeposition method was suggested by Yang *et al.*<sup>84</sup> for the synthesis of bimetallic SnBi catalysts. They utilized the specifically formulated electrolyte solution with an adjusted pH of 8–10 at the temperature of 60 °C to obtain a desirable alloy with the best performance for CO<sub>2</sub> reduction. This group reported a high formate FE of 96.1% at -1.06 V *vs.* RHE for a Sn<sub>0.5</sub>Bi catalyst (0.5 Sn<sup>2+</sup>/Bi<sup>3+</sup> molar ratio), which was attributed to a large surface area with an abundance of active sites and defects. It was reported that the tin metal oxide/bismuth metal oxide interface stabilized the CO<sub>2</sub><sup>-</sup> intermediate and suppressed HER. Also, the electronic coupling at the interfaces of Sn and Bi led to the \*OCHO formation pathway, thus promoting the formate generation. Xu *et al.*<sup>85</sup> prepared a Sn-doped Bi nanowire bundle (NB) through the *in situ* reconstruction of Sn-doped Bi<sub>2</sub>S<sub>3</sub> precursors. By optimizing the doping concentration, a remarkable performance for CO<sub>2</sub>RR to formate could be achieved. The Sn<sub>1/24</sub>-Bi NBs showed a high FE of formate >90% over a wide potential window of -0.5 to -1.9 V *vs.* RHE. The excellent activity of the Sn<sub>1/24</sub>-Bi NBs catalysts originated from the electron-rich surface, as well as a lower reaction kinetic barrier. The calculation of the Fermi level of both Bi and Sn<sub>1/24</sub>-Bi catalysts exhibited the availability of more free electrons on the surface of Sn<sub>1/24</sub>-Bi catalyst, improving the CO<sub>2</sub><sup>-</sup> adsorption.

Zhou *et al.*<sup>87</sup> synthesized a defective BiIn catalyst and studied the influences of defective surfaces on the promotion

of HCOOH formation, showing that the introduction of indium to bismuth is an effective approach to enhance the FE of formate *via* the optimization of the binding energy of \*OCHO. Phosphorus-doped BiIn was used as a pre-catalyst to create defective surfaces during the self-reconstruction. It was demonstrated that the defective sites increased \*OH adsorption, promoted water dissociation, and enhanced CO<sub>2</sub>-RR kinetics. The Bi:In ratio in BiIn catalysts can be optimized to attain high activity and selectivity. For this purpose, Wang *et al.*<sup>88</sup> prepared Bi-In<sub>2</sub>O<sub>3</sub> nanoflower catalysts with different Bi/In ratios and investigated the relationship between the catalyst composition and CO<sub>2</sub>RR performance. It was found that the catalyst with a Bi/In ratio of 6:94 had a high FE of formate (88.1%) at -0.7 V *vs.* RHE. Likewise, indium-bismuth nanosphere catalysts with different compositions were synthesized by Tan *et al.*<sup>30</sup> and tested for CO<sub>2</sub>RR to formate. The In<sub>16</sub>Bi<sub>84</sub> had the highest FE (~100%) of formate at -0.94 V *vs.* RHE as seen in Fig. 5b. It was concluded that the presence of Bi enabled electrons to flow from Bi to In and provided additional active sites for CO<sub>2</sub>RR. Improvements in the performance of bimetallic BiIn catalysts *via* defect engineering were proposed by Yang *et al.*<sup>89</sup> The researchers showed that the oxygen vacancies originating from the lattice mismatches of Bi<sub>2</sub>O<sub>3</sub> and In<sub>2</sub>O<sub>3</sub> could reduce the CO<sub>2</sub> activation energy. DFT calculations confirmed that CO<sub>2</sub> molecules were mainly adsorbed by the oxygen vacancies, and the dominant pathway was through oxygen vacancies. MOF-derived Bi/In bimetallic oxide nanoparticles embedded in carbon networks showed excellent selectivity for formate due to the high surface area, desirable pore size distribution, and high electrical conductivity of the carbon network as well as the synergistic effect of Bi and In bimetallic components.<sup>90</sup>

As a nonprecious earth-abundant metal, Zn is a promising electrocatalyst for CO<sub>2</sub>RR. Recently, the synergistic effects of Zn and Bi have been recognized, and bimetallic ZnBi catalysts have been studied for the CO<sub>2</sub>RR to formate.<sup>91</sup> Wang *et al.*<sup>31</sup> synthesized a Zn-Bi bimetallic catalyst (Zn-Bi<sub>2</sub>O<sub>3</sub>/CN) and revealed that the surface Bi-O structure and synergistic Zn-Bi effect might enhance the CO<sub>2</sub>RR. DFT calculations indicated that the presence of Zn reduced the energy barrier of HCOO\* formation, thus facilitating the production of formate. A hydrothermal process was employed by Zhang *et al.*<sup>91</sup> to prepare bimetallic ZnBi catalysts with a formate FE of 94% at -0.8 V *vs.* RHE. A feasible and cost-effective strategy was proposed by Sabouhanian *et al.*<sup>86</sup> to grow bismuth nanodendrites on the Zn surface. The ZnBi catalysts were synthesized by immersing the electrodeposited Zn in a bismuth nitrate solution. Due to differences in the reduction potentials of Zn<sup>2+</sup> and Bi<sup>3+</sup>, galvanic replacement took place and Bi nanodendrites grew uniformly on the surface (Fig. 5c). Fig. 5d depicts the activities of Zn and ZnBi electrodes for CO<sub>2</sub>RR (solid lines) and HER (dashed lines). It was observed that the CO<sub>2</sub>RR activity increased significantly after 60 s of immersion (ZnBi-1) and was boosted further at 90 s (ZnBi-2). After 90 s, the CO<sub>2</sub>RR was only slightly improved for 120 s of



the galvanic replacement time (ZnBi-3). Furthermore, the additional incorporation of Bi decreased the onset potential for CO<sub>2</sub>RR. In contrast, the HER activity remained almost the same by introducing Bi as a secondary element. *In situ* IR spectroscopy determined that CO<sub>2</sub> reduction at the ZnBi catalysts proceeded through the generation of the adsorbed \*COO<sup>-</sup> intermediate.

### 3.2. Generation of other products

Although most of the reported bimetallic CuBi catalysts exhibited high selectivity for the production of formate, recent research has suggested the feasibility of generating other products.<sup>32</sup> Azenha *et al.*<sup>92</sup> reported the deposition of Bi on CuO NWs under various charge levels passed through the substrate; the formed catalyst demonstrated an exceptionally high selectivity of CO<sub>2</sub>RR for the generation of propane in a 0.1 M KHCO<sub>3</sub> electrolyte, which achieved an FE of 85.4% (Fig. 6a). This remarkable catalytic performance was attributed to enhanced CO<sub>2</sub> and CO adsorption capacities due to abundant oxygen defects. In another study, Wang *et al.*<sup>32</sup> developed bimetallic Cu<sub>x</sub>Bi aerogel catalysts by simultaneously reducing CuCl<sub>2</sub>·2H<sub>2</sub>O and BiCl<sub>3</sub> with NaBH<sub>4</sub>, and controlled the composition of Cu<sub>x</sub>Bi aerogels where X was 5, 10, 50, and 100. Interestingly, the product selectivity varied from CO to CH<sub>4</sub>, C<sub>2</sub>H<sub>4</sub>, or formate. A schematic for the synthesis of Cu<sub>x</sub>Bi aerogels with different selectivity is presented in Fig. 6b. It was demonstrated that the introduction of varying amounts of Bi resulted in changes to the Cu(II)/Cu(I) ratios on the catalyst surface; thus, regulating the hydrogenation capacities of intermediates. Similarly, Cu-Bi NPs were prepared with different stoichiometric ratios *via* chemical reduction, which revealed that the FE of CH<sub>4</sub> and C<sub>2</sub>H<sub>4</sub> was sensitive to the quantity of Bi.<sup>93</sup> Cu<sub>7</sub>Bi<sub>1</sub> had a high FE (70.6%) for CH<sub>4</sub> at -1.2 V (*vs.* RHE). Further, lowering the C-C coupling energy barrier to enhance the FE of C<sub>2</sub>H<sub>4</sub> was verified through the integration of single Bi atoms and oxygen vacancies with CuO (Bi-CuO (V<sub>O</sub>)).<sup>33</sup> Interestingly, Bi-

CuO (V<sub>O</sub>) with a FE that exceeded 48% of C<sub>2</sub>H<sub>4</sub> at -1.05 V (*vs.* RHE) significantly outperformed the other Cu-based electrocatalysts. Cao *et al.*<sup>94</sup> further showed the C-C coupling ability of a single Bi atom-decorated Cu alloy (BiCu-SAA) by employing operando FTIR based on a synchrotron radiation (SR-FTIR) technique. The appearance of an absorption peak at 1563 cm<sup>-1</sup> corresponded to the \*COCOH species, which verified the C-C coupling for C<sub>2</sub> products.

## 4. *In situ* spectroscopic studies

The Bi-based catalysts were often synthesized through the *in situ* electrochemical transformation of the initial Bi-containing precursors. Thus, it is vital to monitor and understand the *in situ* structural reconstruction during the CO<sub>2</sub>RR. *In situ* Raman spectroscopy has been employed to monitor the dynamic reconstruction and evolution of Bi-based catalysts under CO<sub>2</sub>RR conditions.<sup>95</sup> The transformation of the initial Bi-containing precursors to Bi NPs can be explored *via in situ* Raman spectroscopy through changes in the Raman peaks assigned to the vibration of the Bi-M or Bi-O bonds.<sup>36</sup> Shen *et al.*<sup>39</sup> showed the structural reconstruction of the CuS-Bi<sub>2</sub>S<sub>3</sub> precursor to metallic Bi. *In situ* Raman spectra revealed that the band assigned to Bi<sub>2</sub>S<sub>3</sub> and CuS quickly disappeared and two broad bands at 72 and 96 cm<sup>-1</sup> appeared, which were ascribed to the E<sub>g</sub> and A<sub>1g</sub> stretching modes of Bi-Bi bonds. Although most studies have shown the complete reduction of Bi<sub>2</sub>O<sub>3</sub> to metallic Bi during the CO<sub>2</sub> reduction, Deng *et al.*<sup>96</sup> demonstrated the partial reduction of Bi<sub>2</sub>O<sub>3</sub> by *in situ* Raman spectroscopy. They reported that the presence of Bi-O structure at the near surface was the main incentive for the selective conversion of CO<sub>2</sub> to formate. The Bi-O structure could enhance CO<sub>2</sub> adsorption and improve the stabilization of CO<sub>2</sub><sup>-</sup> intermediate.

The formation of bismuth subcarbonate (Bi<sub>2</sub>O<sub>2</sub>CO<sub>3</sub>) was reported and detected by *in situ* Raman spectroscopy during the CO<sub>2</sub>RR, contingent on the electrolyte and initial

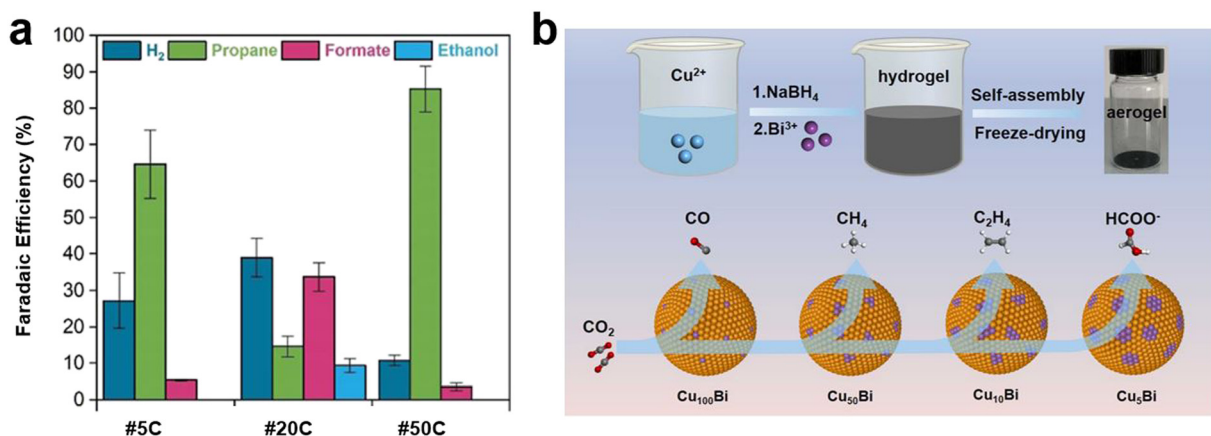
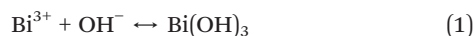


Fig. 6 (a) Faradaic efficiencies of CO<sub>2</sub>RR on CuBi catalysts prepared with different charge values passed through the substrate using 0.1 M KHCO<sub>3</sub> catholyte<sup>92</sup> (copyright 2022 Elsevier); (b) schematic of synthesis procedure for Cu<sub>x</sub>Bi aerogels and different product selectivity<sup>32</sup> (copyright 2022 Elsevier).



composition of the Bi precursor.<sup>95</sup> An *et al.*<sup>97</sup> reported that the formation of  $\text{Bi}_2\text{O}_2\text{CO}_3$  originated from the formation of a surface oxide layer ( $\text{Bi}^{3+}$ ) or oxidized metal Bi exposed to air ( $\text{BiO}^+$ ). In the case of  $\text{Bi}^{3+}$  formation, bismuth hydroxide ( $\text{Bi}(\text{OH})_3$ ) was generated by the reaction of the  $\text{Bi}^{3+}$  and  $\text{OH}^-$  from local alkalinity. However, the  $\text{Bi}(\text{OH})_3$  was not stable and reacted with  $\text{CO}_2$  to form  $\text{Bi}_2\text{O}_2\text{CO}_3$  as shown in reaction (1) and (2). In the case of  $\text{BiO}^+$  formation, it further reacted with carbonate that was present in the highly alkaline  $\text{CO}_2$ -purged electrolyte to form  $\text{Bi}_2\text{O}_2\text{CO}_3$  species as shown in reaction (3) and (4).



The existence of  $\text{Bi}_2\text{O}_2\text{CO}_3$  species during the  $\text{CO}_2\text{RR}$  process was detected using the *in situ* shell-isolated

nanoparticle enhanced Raman spectroscopy (SHINERS) method. The appearance of the Bi–O stretching vibration of  $\text{Bi}_2\text{O}_2\text{CO}_3$  located at  $182\text{ cm}^{-1}$  confirmed the formation of  $\text{Bi}_2\text{O}_2\text{CO}_3$  on the electrode surface.<sup>95</sup> Wu *et al.*<sup>38</sup> demonstrated that a thin layer of  $\text{Bi}_2\text{O}_2\text{CO}_3$  initially formed on the surface; however, it could be completely diminished and converted to metallic Bi prior to the occurrence of  $\text{CO}_2\text{RR}$ . As shown in Fig. 7a, the peak at  $162\text{ cm}^{-1}$  assigned to the Bi=O vibration mode of the  $\text{Bi}_2\text{O}_2\text{CO}_3$  appeared at the open circuit potential (OCP), which verified the formation of the  $\text{Bi}_2\text{O}_2\text{CO}_3$ . With the application of more negative potentials from OCP to  $-0.9\text{ V}$ , the peak intensity decreased and finally disappeared. Similarly, the transformation of  $\text{Bi}_2\text{O}_3$  microcrystals to  $\text{Bi}_2\text{O}_2\text{CO}_3$  under electrochemical conditions was reported by Zeng *et al.*,<sup>98</sup> it was further reduced to metallic Bi at potentials higher than  $-0.6\text{ V vs. RHE}$ .  $\text{Bi}_2\text{O}_2\text{CO}_3$  has also been directly employed as a catalyst for  $\text{CO}_2\text{RR}$ .<sup>57,70</sup> The abundant oxygen vacancies in  $\text{Bi}_2\text{O}_2\text{CO}_3$  nanosheets ( $\text{V}_\text{O}$ -BOC-NS) served as durable electrocatalysts for  $\text{CO}_2$  reduction to formate with an FE of  $>95\%$  at  $-0.62\text{ V vs. RHE}$ . The stability of the  $\text{V}_\text{O}$ -BOC-NS catalyst under  $\text{CO}_2$  reduction conditions was characterized using *in situ* Raman spectroscopy in a  $0.5\text{ M}$

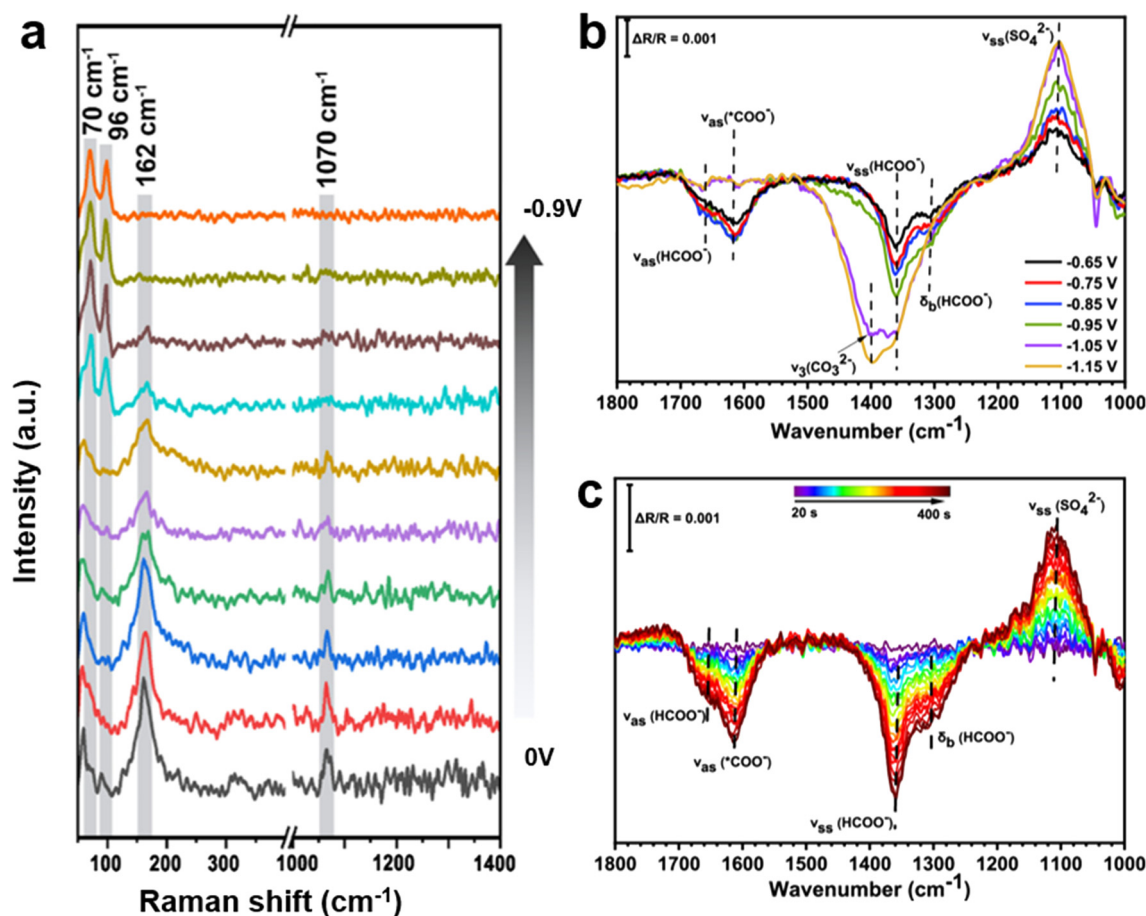


Fig. 7 (a) *In situ* Raman spectra for the transformation of the  $\text{Bi}_2\text{O}_3$  precursor from  $\text{Bi}_2\text{O}_2\text{CO}_3$  to Bi during the  $\text{CO}_2\text{RR}$ <sup>38</sup> (copyright 2022 American Chemical Society); potential-dependent (b) and time-dependent (c) IR spectra measured in a  $\text{CO}_2$ -saturated  $0.1\text{ M K}_2\text{SO}_4$  solution for the ZnBi-3 electrode<sup>86</sup> (copyright 2024 American Chemical Society).



KCl electrolyte. No notable change of the intensity of peak at  $1066\text{ cm}^{-1}$  derived from  $\text{CO}_3^{2-}$  in  $\text{V}_\text{O}$ -BOC-NS was observed even at more negative potentials, showing excellent stability.<sup>99</sup>

In addition to studying the structural evolution of materials, the detection of key intermediates and the elucidation of reaction pathways are vital for gaining better insights into reaction mechanisms, and further improving performance by modifying the binding energy of intermediates.<sup>100</sup> It was reported that the generation of formate often occurs through the oxygen-bridged  $^*\text{OCHO}$  intermediate on Bi-based catalysts.<sup>57,76</sup> The stability of the adsorbates with Bi–O bonds is systematically higher than those with C–Bi bonds. Thus, the  $^*\text{OCHO}$  pathway is dominant compared with  $^*\text{COOH}$  pathway, leading to higher selectivity of formate generation. Some studies have shown that the formation of the  $^*\text{OCHO}$  intermediate is accompanied by the adsorption of  $\text{HCO}_3^-$  groups.<sup>101</sup> Sabouhanian *et al.*<sup>86</sup> studied the  $\text{CO}_2$  reduction mechanism at ZnBi catalysts using an *in situ* electrochemical ATR-FTIR technique. As shown in Fig. 7b, the peaks assigned to formate at  $1305\text{ cm}^{-1}$  (C–H bending mode),  $1360\text{ cm}^{-1}$  (C–O symmetric stretch), and  $1660\text{ cm}^{-1}$  (C=O asymmetric stretch) were observed. The signal that appeared at  $1614\text{ cm}^{-1}$  was attributed to the asymmetric stretch of the adsorbed  $^*\text{COO}^-$  intermediate, revealing that the  $\text{CO}_2$  molecule was adsorbed by the carbon atom in a monodentate orientation. The time-dependent FTIR spectra of the ZnBi catalyst are presented in Fig. 7c to monitor the formation and consumption of species over time. It was observed that the peaks assigned to the

symmetric and asymmetric stretches of formate followed the same trend as the peak allocated to  $^*\text{COO}^-$ , and they became stronger as the reaction progressed. This proves that more  $^*\text{COO}^-$  species resulted in the production of more formate.

## 5. Industrial perspective

Although Bi-based catalysts exhibit a high FE and selectivity for formate, the required high activity, high stability, and low overpotential hinder them from being employed on an industrial scale. Consequently, multiple challenges need to be resolved in terms of their stabilities and activities for industrial applications.<sup>34,39</sup> To meet the required criteria for commercialization, it is necessary to achieve current densities of  $>200\text{ mA cm}^{-2}$  and long-term ( $>100\text{ h}$ ) stability.<sup>16</sup> Encouraging progress has been made recently toward upgrading the electrochemical stability of Bi-based catalysts, while maintaining high activity. Flow cells and membrane electrode electrolyzers were developed for scalable  $\text{CO}_2\text{RR}$  systems as they can address mass transport issues.<sup>77,102,103</sup> The gas diffusion electrode (GDE) configuration allowed  $\text{CO}_2$  to access the electrode surface as a gas and facilitated its mass transportation. There are some pending patents using Bi-based catalysts for  $\text{CO}_2$  reduction to formate.<sup>104,105</sup> A superior high current density of  $2.0\text{ A cm}^{-2}$  with 93% FE of formate at  $-0.95\text{ V vs. RHE}$  (Fig. 8a) was achieved by Lin *et al.*<sup>63</sup> in a flow cell. This group synthesized a  $\text{Bi}_2\text{S}_3$  precursor that underwent structural evolution and created a nanocomposite catalyst containing  $\text{Bi}^0$  clusters and  $\text{Bi}_2\text{O}_2\text{CO}_3$  nanosheets. They showed that the FE of formate increased

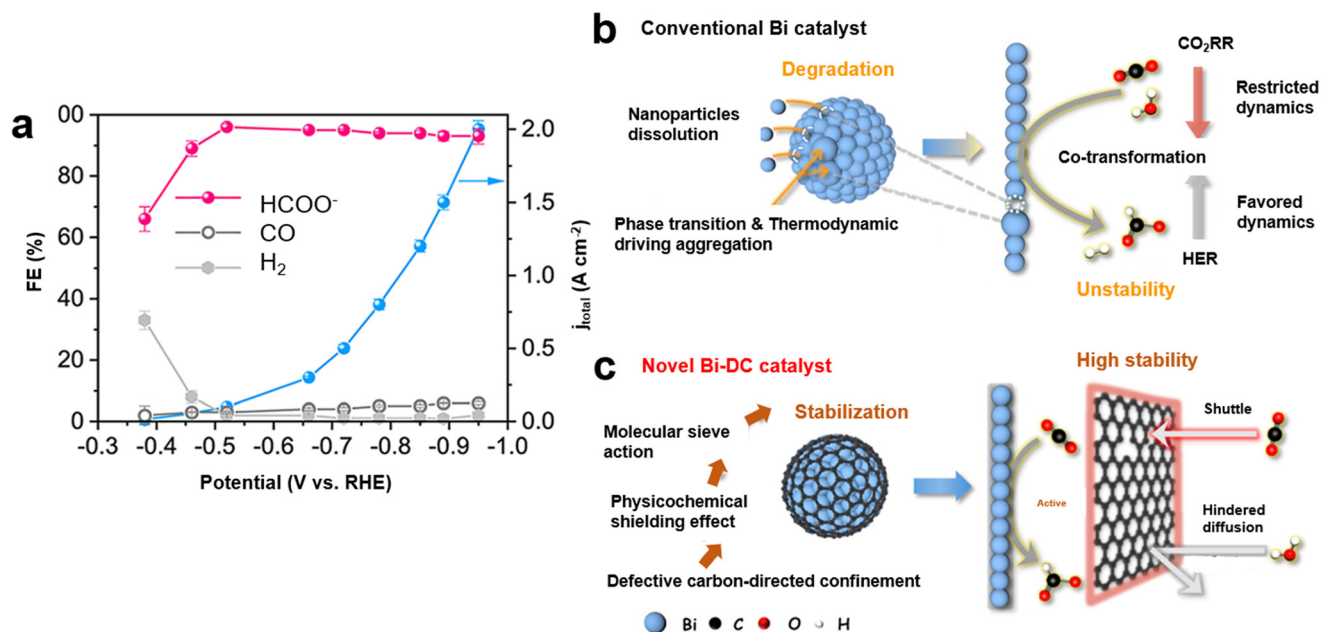


Fig. 8 (a) The measured FE of each product and total current density for  $\text{CO}_2$  reduction over a  $\text{Bi}_2\text{S}_3$ -derived catalyst using 1 M KOH electrolyte in a flow cell<sup>63</sup> (copyright 2023 John Wiley and Sons); (b) schematic of the degradation of a conventional Bi catalyst and limited  $\text{CO}_2\text{RR}$  dynamics; (c) schematic of structural stabilization using a novel Bi-DC catalyst with a special  $\text{sp}^2/\text{sp}^3$  carbon hybridization structure for efficient and stable formate formation<sup>106</sup> (copyright 2024 American Chemical Society).



from 66% at  $-0.38$  V vs. RHE to 96% at  $-0.52$  V vs. RHE. This catalyst maintained a stable and industrial-level current density for 100 h. Interestingly, Shen *et al.*<sup>39</sup> prepared a  $\text{Bi}_2\text{S}_3$ -containing precursor through the integration of CuS. The CuS– $\text{Bi}_2\text{S}_3$  nano-heterojunction precursor was observed to be reconstructed to Cu-doped Bi (CDB) nanosheet electrocatalysts. An industrial-compatible current density of  $-1132$  mA  $\text{cm}^{-2}$  at  $-0.86$  V vs. RHE was recorded in a flow cell. Moreover, the long-term stability of over 100 h at  $-400$  mA  $\text{cm}^{-2}$  was attained in a membrane electrode assembly.

In addition to the activity, stability is the most important issue for Bi-based catalysts due to thermodynamically driven aggregation of nanoparticles, the dissolution of reactive species, and structural reconstruction during  $\text{CO}_2\text{RR}$ .<sup>39,45,106</sup> Only a few research papers have reported a stability time of  $\sim 100$  h. As catalytic reactions take place on the catalyst's surface, surface modifications can greatly influence the catalytic reactions. The microenvironmental modulation using the molecularly modified surface layers can impact the adsorption behavior of ions and molecules on the catalyst, improving the stability during  $\text{CO}_2$  reduction.<sup>107</sup> For example, HER on Cu nanoneedles was suppressed by a hydrophobic polytetrafluoroethylene (PTFE) coating, leading to the high  $\text{C}_2$  selectivity with 47% FE. Moreover, the Cu nanoneedle structures were well maintained during the  $\text{CO}_2$  reduction due to the PTFE coating, resulting in high stability.<sup>108</sup> Li *et al.*<sup>106</sup> recorded the most prolonged stability (120 h at 0.4 A) in a membrane electrode assembly cell. A  $\text{CO}_2$ -philic defective carbon (DC) was formed over a Bi catalyst (Bi-DC), where the presence of  $\text{sp}^3$ -hybrid defects in the carbon exhibited a unique sieving effect on  $\text{CO}_2$  molecules. Thus, it could effectively suppress the degradation and structural evolution of active Bi species during  $\text{CO}_2\text{RR}$ . The DC species facilitated the formation of an interconnected carbon network, which enhanced the dispersion of the active Bi component. This resulted in a larger electrochemical surface area (ECSA) and, consequently, a higher current density. Schematics of the degradation of a conventional Bi catalyst and structural stabilization using a novel Bi-DC catalyst are presented in Fig. 8b and c, respectively. It has been reported that the stability of the Bi-based catalysts might be affected by the oxygenated species from the electrolyte leading to poisoning of the active sites. Zhu *et al.*<sup>107</sup> introduced a molecular passivation layer of oxyphilic ascorbic acid to inhibit the poisoning of the hydroxyl. So, the free  $\text{OH}^-$  preferred to bind to the outer ascorbic acid layer, and the possibility of binding to defective Bi sites was reduced. As a result, the high stability of over 120 hours was achieved at 50 mA  $\text{cm}^{-2}$ . It has been reported that liquid metals as catalysts might have higher stability compared with solid ones due to dynamic surface properties and surface renewal ability. Liquid Bi alloy catalysts were generated by Guo *et al.*,<sup>109</sup> showing 98% FE of formate over 80 h. They overcame the problem of deterioration of the traditional solid-state Bi-based catalysts during  $\text{CO}_2$  reduction. Compared with the liquid Bi alloy, the solid one exhibited a lower formate FE and less stability. To

date, alkaline electrolytes have exhibited the highest activity for  $\text{CO}_2\text{RR}$  to formate using Bi-based catalysts.<sup>110</sup> For example, Peng *et al.*<sup>111</sup> demonstrated that KOH solutions had improved activities over  $\text{KHCO}_3$  due to their lower solution resistance, which was confirmed by EIS. However,  $\text{CO}_2$  molecules can react with  $\text{OH}^-$  ions in alkaline electrolytes and be converted to carbonate, which leads to carbonate deposition and the consumption of  $\text{CO}_2$  feedstocks.<sup>112</sup> More importantly, the formation of carbonates can significantly threaten the stability of  $\text{CO}_2\text{RR}$ , as they may obstruct the porous channels required for  $\text{CO}_2$  transport in the gas diffusion electrode, accelerate electrolyte leakage and raise cell resistance. These challenges greatly constrain the industrial potential of an alkaline or neutral  $\text{CO}_2\text{RR}$  system.<sup>113</sup> Recently, Bi-based catalysts have been utilized for  $\text{CO}_2\text{RR}$  in acidic electrolytes to overcome the aforementioned issues. Formic acid is generated in acidic electrolytes rather than formate, which can reduce the industrial expenses associated with subsequent separation and purification from the electrolyte.<sup>20</sup> However, HER typically dominates under acidic conditions. For example, in a strong acid with a pH of 1 or lower, the FE for  $\text{CO}_2\text{RR}$  products is nearly zero.<sup>113</sup> Recently, a strategy for the engineering of the local microenvironment has been proposed to enhance the  $\text{CO}_2\text{RR}$  under acidic conditions. It was found that the HER in acidic electrolytes could be suppressed by creating a hydrophobic interfacial environment,<sup>112</sup> or reducing proton coverage<sup>113</sup> on the catalyst surface. The FE of formate up to 92.2% at a current density of  $-237.1$  mA  $\text{cm}^{-2}$  was reported for  $\text{CO}_2$  reduction over Bi NSs in acidic electrolytes.<sup>113</sup> The recently reported Bi-based catalysts with an industrially compatible current density of formate are summarized in Table 1, showing that over 90% FE was achieved.

## 6. Conclusions and perspectives

The recent advances in Bi-based catalysts for  $\text{CO}_2$  reduction are compared in Table 2 and Fig. 9, which highlight various morphologies and structures obtained for Bi-based catalysts along with their FE of formate. Bi-based catalysts have shown a high FE and selectivity for the generation of formate and may serve in the future as a potential electrocatalyst for  $\text{CO}_2\text{RR}$  to formate for industrial applications. Through innovative synthesis techniques and the careful engineering of catalyst structures, researchers have achieved remarkable advancements to improve the activity and selectivity. Further, the introduction of secondary elements to synthesize bimetallic Bi-based catalysts has been extensively studied to decrease the energy barrier for intermediate formation. Not only formate but also other products such as propane, methane, and ethylene could be produced using CuBi catalysts by regulating the hydrogenation capacities of intermediates, enhancing  $\text{CO}_2$  and CO adsorption capacities, and lowering the C–C coupling energy barrier. Significant advances have been made using flow cell and membrane electrode assembly



**Table 1** Recently reported Bi-based catalysts with industrially compatible current densities of formate

Catalyst	Electrolyte	Potential (V vs. RHE)	Current density (mA cm <sup>-2</sup> )	Stability (h)	FE (%)	Ref.
Ti-Bi NS	1 M KOH	-1.01	224.1	12	96.3	69
Heterophase Bi	1 M KOH	-0.68	140	10	95.2	114
Cu@Bi NW/Cu	0.5 M KHCO <sub>3</sub>	-1.07	129	6	98.7	42
BOC@GDY	1 M KOH	-1.1	200	10	93.5	115
Bi NS	1 M KOH	-0.63	400	26	>90	19
Bi-ene-NW	1 M KOH	-0.7	200	110	>90	16
In/Bi-750	1 M KOH	-1.2	200	13	90.8	26
Bi-GDE	1 M KOH	-1.2	355	60	94	98
BiIn@P	1 M KOH	-0.92	500	17	97.3	87
BOC-NS	1 M KOH	-1.55	1000	24	93	116
Copper-doped bismuth	5 M KOH	-0.86	1132	100	>90	39
Sn <sub>1/24</sub> -Bi	1 M KOH	-0.5-1.9	>200	84	>90	85
Bi <sub>2</sub> S <sub>3</sub> -derived	1 M KOH	-0.95	2000	100	93	63

**Table 2** Comparison between the performance of different Bi-based catalysts recently reported in the literature for the conversion of CO<sub>2</sub>RR to formate

	Catalyst	Synthesis method	Electrolyte	Potential (RHE)	Stability (h)	FE (%)	Ref.	
Mono-metallic Bi-based	Bi NS	Electroreduction	0.5 M KHCO <sub>3</sub>	-0.8--1.2	22	90	38	
	OD-BiNS	Electrochemical transformation	0.5 M KHCO <sub>3</sub>	-0.95	10	93	21	
	Bi-PNS	Solvothermal	0.5 M KHCO <sub>3</sub>	-1.0	9	95	59	
	Bi NS	Electroreduction	0.5 M KHCO <sub>3</sub>	-0.98	12	94.5	36	
	Bi-S	Electrochemical transformation	0.5 M KHCO <sub>3</sub>	-0.9	35	96.7	66	
	Bi PNS	Electroreduction	0.1 M KHCO <sub>3</sub>	-1.2	10	95.31	61	
	Bi <sub>2</sub> S <sub>3</sub> /CNTs	Sonochemical	0.5 M KHCO <sub>3</sub>	-0.91	78	99.3	117	
	Bi/BiO <sub>x</sub> NS	Electrochemical conversion	0.5 M KHCO <sub>3</sub>	-0.78--1.18	10	94	48	
	Bi-metallic Bi-based	CuBi	Co-deposition	0.5 M KHCO <sub>3</sub>	-0.97	20	94.4	73
		Bi-Cu (2:1)	Ion-assisted codeposition	0.1 M KHCO <sub>3</sub>	-1.0	20	94.1	74
Cu-Bi aerogel		One-step reduction	0.5 M KHCO <sub>3</sub>	-0.9	36	96.57	81	
Cu <sub>0.8</sub> Bi <sub>0.2</sub>		Thermal evaporation	1 M KOH	~-0.72	24	>95	118	
Bi <sub>3</sub> Cu <sub>1</sub>		Hydrothermal	0.5 M KOH	-0.75	20	95.1	77	
P-Cu-BiNF		Fast reduction	0.5 M KHCO <sub>3</sub>	-0.78--1.08	12	90	119	
Bi-Cu		Electrochemical deposition	0.5 M KHCO <sub>3</sub>	-0.91	50	94.37	111	
CuBi		CuBi-MOF	0.5 M KHCO <sub>3</sub>	-0.77	24	100	82	
Bi on Cu foil		Electrodeposition	0.1 M KHCO <sub>3</sub>	-0.65	24	100	120	
Cu@Bi nanocone		Electrodeposition	0.5 M KHCO <sub>3</sub>	-0.95	10	96.9	98	
Bi/Cu foam		Electrodeposition	0.1 M KHCO <sub>3</sub>	-1.0	20	92	97	
Cu <sub>1</sub> Bi <sub>1</sub>		Co-precipitation	0.5 M KHCO <sub>3</sub>	-0.98	60	98.07	83	
Bi <sub>5</sub> Sn <sub>60</sub>		Electrodeposition	0.1 M KHCO <sub>3</sub>	-1.0	20	94.8	29	
Bi-Sn aerogel		Chemical reduction	0.1 M KHCO <sub>3</sub>	-1.0	10	93.9	99	
Sn-doped Bi <sub>2</sub> O <sub>3</sub> NSs		Solvothermal	0.5 M KHCO <sub>3</sub>	-0.97	8	93.4	121	
SnBi		Electrodeposition	0.5 M KHCO <sub>3</sub>	-1.06	100	96.1	84	
Sn-Bi		Hydrothermal	0.5 M KHCO <sub>3</sub>	-0.74--1.14	160	>90	122	
Sn <sub>1-x</sub> Bi <sub>x</sub>		Co-reduction	0.5 M KHCO <sub>3</sub>	-0.67--0.92	50	>90	123	
In/Bi-750		Electrochemical transformation	0.5 M KHCO <sub>3</sub>	-1.0	48	97.17	26	
BiIn <sub>5</sub> -500@C		MOF	0.5 M KHCO <sub>3</sub>	-0.86	15	97.5	124	
Bi-In <sub>2</sub> O <sub>3</sub>	Wet chemical	0.5 M KHCO <sub>3</sub>	-0.7	10	88.1	88		
In <sub>16</sub> Bi <sub>84</sub> NS	Liquid-polyol	0.5 M KHCO <sub>3</sub>	-0.94	10	~100	30		
In <sub>2</sub> O <sub>3</sub> /Bi <sub>2</sub> O <sub>3</sub>	MOF	0.5 M KHCO <sub>3</sub>	-0.4--1.6	30	99.9	89		
Zn-Bi	Hydrothermal	0.5 M NaHCO <sub>3</sub>	-0.8	7	94	91		

electrolyzers utilizing gas-diffusion electrodes to achieve high current densities owing to rapid mass transfer. Selectivity of up to 100% and current densities higher than -200 mA cm<sup>-2</sup> have been reached in most recent studies. However, achieving ampere-level current densities and long-term stabilities of >100 h remains challenging. Consequently, despite several notable achievements, there is still a need to direct future research as follows to narrow the gap between laboratory and industrial scales.

Continued efforts should be made to enhance the stability of Bi-based catalysts for industrial applications. It is also necessary to conduct further research into scalable synthesis techniques and cost-effective catalyst design for large-scale applications. It is vital to gain insights into the kinetics of CO<sub>2</sub>RR and identify intermediates in real-world applications. Thus, *in situ* characterization techniques should be developed to be compatible with high current densities. Further research should be conducted to optimize the conditions and



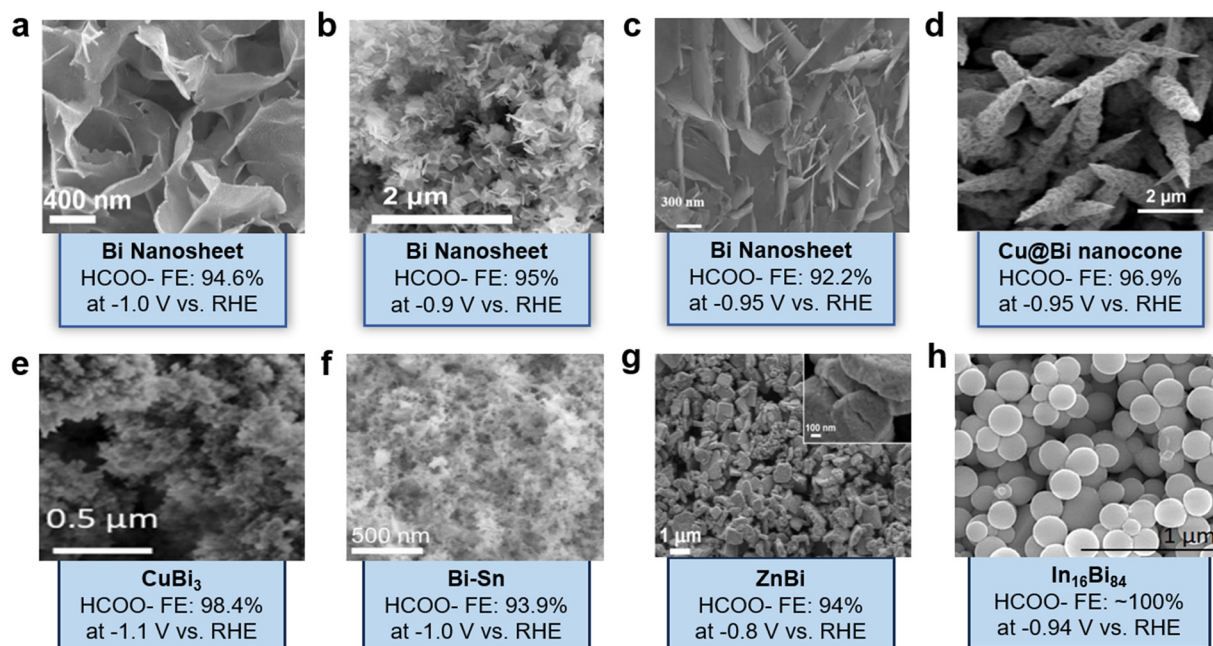


**Fig. 9** SEM images of (a) Bi NSs<sup>38</sup> (copyright 2022 American Chemical Society); (b) P-nanoplates-Bi catalysts<sup>40</sup> (copyright 2021 Elsevier); (c) nitrogen-doped Bi NSS<sup>125</sup> (copyright 2022 MDPI); (d) Cu@Bi nanocone<sup>126</sup> (copyright 2020 Elsevier); (e) CuBi<sub>3</sub> (ref. 71) (copyright 2023 Elsevier); (f) Bi-Sn aerogel<sup>127</sup> (copyright 2021 John Wiley and Sons); (g) ZnBi (ref. 91) (copyright 2024 American Chemical Society); (h) In<sub>16</sub>Bi<sub>84</sub> (ref. 30) (copyright 2022 American Chemical Society).

designs of cells to generate concentrated formic acid to reduce the expenses of product purification and separation. Integrating Bi-based catalysts with renewable energy sources such as solar and wind power should be considered. The coupling of electrochemical CO<sub>2</sub> reduction with renewable energy will reduce the reliance on fossil fuels and contribute to a greener energy landscape. Finally, CO<sub>2</sub>RR should be assessed regarding the economic perspective and environmental impact. Building a pilot-scale system that allows for real-world testing is crucial to evaluating the stability of the catalysts, the costs and the efficiency of the CO<sub>2</sub> reduction process. It would provide valuable data on operational expenses, overall system performance, and long-term durability, offering key insights into the economic viability and potential scalability.

## Data availability

This is a review article. All the data are extracted from the published papers, which are specially described in the related figures and tables.

## Conflicts of interest

There are no conflicts to declare.

## Acknowledgements

This research was funded by Discovery Grants from the Natural Sciences and Engineering Research Council of Canada (J.L.: RGPIN-2022-03958; A.C.: RGPIN-2022-04238). A.

C. acknowledges the NSERC and Canada Foundation for Innovation (CFI) for the Canada Research Chair Award in Electrochemistry and Nanoscience.

## References

- 1 S. Abner and A. Chen, Design and mechanistic study of advanced cobalt-based nanostructured catalysts for electrochemical carbon dioxide reduction, *Appl. Catal., B*, 2022, **301**, 120761.
- 2 A. Salverda, S. Abner, E. Mena-Morcillo, A. Zimmer, A. Elsayed and A. Chen, Electrochemical, scanning electrochemical microscopic, and in situ electrochemical fourier transform infrared studies of CO<sub>2</sub> reduction at porous copper surfaces, *J. Phys. Chem. C*, 2023, **127**, 7151–7161.
- 3 Y.-X. Duan, R.-C. Cui and Q. Jiang, Recent progress on the electroreduction of carbon dioxide to C<sub>1</sub> liquid products, *Curr. Opin. Electrochem.*, 2023, **38**, 101219.
- 4 P. Roy, A. K. Mohanty and M. Misra, Prospects of carbon capture, utilization and storage for mitigating climate change, *Environ. Sci.:Adv.*, 2023, **2**, 409–423.
- 5 Q. Zhu, Y. Zeng and Y. Zheng, Overview of CO<sub>2</sub> capture and electrolysis technology in molten salts: operational parameters and their effects, *Ind. Chem. Mater.*, 2023, **1**, 595–617.
- 6 X. Li, X. Wu, X. Lv, J. Wang and H. B. Wu, Recent advances in metal-based electrocatalysts with hetero-interfaces for CO<sub>2</sub> reduction reaction, *Chem Catal.*, 2022, **2**, 262–291.



- 7 Z. Yang, R. Chen, L. Zhang, Y. Li and C. Li, Recent progress in nickel single-atom catalysts for the electroreduction of CO<sub>2</sub> to CO, *Ind. Chem. Mater.*, 2024, 2, 533–555.
- 8 W. Chen, Y. Wang, Y. Li and C. Li, Electrocatalytic CO<sub>2</sub> reduction over bimetallic Bi-based catalysts: A review, *CCS Chem.*, 2023, 5, 544–567.
- 9 F. Rahmati, N. Sabouhanian, J. Lipkowski and A. Chen, Synthesis of 3D porous Cu nanostructures on Ag thin film using dynamic hydrogen bubble template for electrochemical conversion of CO<sub>2</sub> to ethanol, *Nanomaterials*, 2023, 13, 778.
- 10 X. Li, Z. Li, Z. Zhang, Y. Zhao, Q. Fang, J. Tang and J. He, Design and synthesis of magnesium-modified copper oxide nanosheets as efficient electrocatalysts for CO<sub>2</sub> reduction, *Nanoscale*, 2024, 16, 17527–17536.
- 11 I. Husein, J. M. Hadi, A. Surendar, N. N. Gryzunova, R. G. Khairullina, D. O. Bokov and H. T. Hoi, Bismuth oxide nanostructure supported on Cu foam as efficient electrocatalyst toward carbon dioxide electroreduction, *Ionics*, 2023, 29, 3213–3223.
- 12 S. Qiao, G. Zhang, D. Tian, W. Xu, W. Jiang, Y. Cao, J. Qian, J. Zhang, Q. He and L. Song, Stepped copper sites coupling voltage-induced surfactant assembly to achieve efficient CO<sub>2</sub> electroreduction to formate, *Energy Environ. Sci.*, 2024, 17, 6779–6786.
- 13 B. Ávila-Bolívar, R. Cepitis, M. Alam, J.-M. Assafrei, K. Ping, J. Aruväli, A. Kikas, V. Kisand, S. Vlassov, M. Käärrik, J. Leis, V. Ivaništštev, P. Starkov, V. Montiel, J. Solla-Gullón and N. Kongi, CO<sub>2</sub> reduction to formate on an affordable bismuth metal-organic framework based catalyst, *J. CO<sub>2</sub> Util.*, 2022, 59, 101937.
- 14 R. Sun, Y. Liao, S.-T. Bai, M. Zheng, C. Zhou, T. Zhang and B. F. Sels, Heterogeneous catalysts for CO<sub>2</sub> hydrogenation to formic acid/formate: from nanoscale to single atom, *Energy Environ. Sci.*, 2021, 14, 1247–1285.
- 15 W. Mao, Q. Yuan, H. Qi, Z. Wang, H. Ma and T. Chen, Recent progress in metabolic engineering of microbial formate assimilation, *Appl. Microbiol. Biotechnol.*, 2020, 104, 6905–6917.
- 16 M. Zhang, W. Wei, S. Zhou, D.-D. Ma, A. Cao, X.-T. Wu and Q.-L. Zhu, Engineering a conductive network of atomically thin bismuthene with rich defects enables CO<sub>2</sub> reduction to formate with industry-compatible current densities and stability, *Energy Environ. Sci.*, 2021, 14, 4998–5008.
- 17 R. Mohan, Green bismuth, *Nat. Chem.*, 2010, 2, 336.
- 18 Y. Guan, M. Liu, X. Rao, Y. Liu and J. Zhang, Electrochemical reduction of carbon dioxide (CO<sub>2</sub>): bismuth-based electrocatalysts, *J. Mater. Chem. A*, 2021, 9, 13770–13803.
- 19 Z. Wang, X. Zu, X. Li, L. Li, Y. Wu, S. Wang, P. Ling, Y. Zhao, Y. Sun and Y. Xie, Industrial-current-density CO<sub>2</sub>-to-formate conversion with low overpotentials enabled by disorder-engineered metal sites, *Nano Res.*, 2022, 15, 6999–7007.
- 20 X.-D. Liang, N. Tian, S.-N. Hu, Z.-Y. Zhou and S.-G. Sun, Recent advances of bismuth-based electrocatalysts for CO<sub>2</sub> reduction: Strategies, mechanism and applications, *Mater. Rep.: Energy*, 2023, 3, 100191.
- 21 J. Lee, H. Liu, Y. Chen and W. Li, Bismuth nanosheets derived by in situ morphology transformation of bismuth oxides for selective electrochemical CO<sub>2</sub> reduction to formate, *ACS Appl. Mater. Interfaces*, 2022, 14, 14210–14217.
- 22 W. Lai, Y. Liu, M. Zeng, D. Han, M. Xiao, S. Wang, S. Ren and Y. Meng, One-step electrochemical dealloying of 3D Bi-continuous micro-nanoporous bismuth electrodes and CO<sub>2</sub>-RR performance, *Nanomaterials*, 2023, 13, 1767.
- 23 D. Xia, H. Yu, H. Xie, P. Huang, R. Menzel, M. M. Titirici and G. Chai, Recent progress of Bi-based electrocatalysts for electrocatalytic CO<sub>2</sub> reduction, *Nanoscale*, 2022, 14, 7957–7973.
- 24 M. Wu, B. Xu, Y. Zhang, S. Qi, W. Ni, J. Hu and J. Ma, Perspectives in emerging bismuth electrochemistry, *Chem. Eng. J.*, 2020, 381, 122558.
- 25 S. Liu, B. Hu, J. Zhao, W. Jiang, D. Feng, C. Zhang and W. Yao, Enhanced electrocatalytic CO<sub>2</sub> reduction of bismuth nanosheets with introducing surface bismuth subcarbonate, *Coatings*, 2022, 12, 233.
- 26 Q. Wang, X. Yang, H. Zang, C. Liu, J. Wang, N. Yu, L. Kuai, Q. Qin and B. Geng, InBi bimetallic sites for efficient electrochemical reduction of CO<sub>2</sub> to HCOOH, *Small*, 2023, 19, 2303172.
- 27 Z. Liu, M. N. Hossain, J. Wen and A. Chen, Copper decorated with nanoporous gold by galvanic displacement acts as an efficient electrocatalyst for the electrochemical reduction of CO<sub>2</sub>, *Nanoscale*, 2021, 13, 1155–1163.
- 28 Z. Zhang, W. Liu, W. Zhang, M. Liu and S. Huo, Interface interaction in CuBi catalysts with tunable product selectivity for electrochemical CO<sub>2</sub> reduction reaction, *Colloids Surf., A*, 2021, 631, 127637.
- 29 Z. Li, Y. Feng, Y. Li, X. Chen, N. Li, W. He and J. Liu, Fabrication of Bi/Sn bimetallic electrode for high-performance electrochemical reduction of carbon dioxide to formate, *Chem. Eng. J.*, 2022, 428, 130901.
- 30 D. Tan, W. Lee, Y. E. Kim, Y. N. Ko, M. H. Youn, Y. E. Jeon, J. Hong, J. E. Park, J. Seo, S. K. Jeong, Y. Choi, H. Choi, H. Y. Kim and K. T. Park, In-Bi electrocatalyst for the reduction of CO<sub>2</sub> to formate in a wide potential window, *ACS Appl. Mater. Interfaces*, 2022, 14, 28890–28899.
- 31 C. Wang, A. He, N. Zhang, H. Sui, Z. Wen, C. Xu, G. Yan and R. Xue, Zn-Bi bimetallic catalyst for electrochemical synthesis of C<sub>1</sub> products by highly selective CO<sub>2</sub> reduction, *J. Catal.*, 2023, 428, 115128.
- 32 Y. Wang, L. Cheng, Y. Zhu, J. Liu, C. Xiao, R. Chen, L. Zhang, Y. Li and C. Li, Tunable selectivity on copper-bismuth bimetallic aerogels for electrochemical CO<sub>2</sub> reduction, *Appl. Catal., B*, 2022, 317, 121650.
- 33 W. Li, L. Li, Q. Xia, S. Hong, L. Wang, Z. Yao, T.-S. Wu, Y.-L. Soo, H. Zhang, T. W. B. Lo, A. W. Robertson, Q. Liu, L. Hao and Z. Sun, Lowering C–C coupling barriers for efficient electrochemical CO<sub>2</sub> reduction to C<sub>2</sub>H<sub>4</sub> by jointly engineering single Bi atoms and oxygen vacancies on CuO, *Appl. Catal., B*, 2022, 318, 121823.



- 34 J. Xu, S. Yang, L. Ji, J. Mao, W. Zhang, X. Zheng, H. Fu, M. Yuan, C. Yang, H. Chen and R. Li, High current CO<sub>2</sub> reduction realized by edge/defect-rich bismuth nanosheets, *Nano Res.*, 2023, **16**, 53–61.
- 35 C.-J. Peng, X.-T. Wu, G. Zeng and Q.-L. Zhu, In situ bismuth nanosheet assembly for highly selective electrocatalytic CO<sub>2</sub> reduction to formate, *Chem. – Asian J.*, 2021, **16**, 1539–1544.
- 36 A. Xu, D. Wei, X. Chen, T. Yang, Y. Huang, H. He and J. Xu, In situ transformation of bismuth-containing precursors into ultrathin bismuth nanosheets for enhanced electrochemical CO<sub>2</sub> reduction, *Chem. Eng. J.*, 2023, **452**, 139227.
- 37 L. Lv, R. Lu, J. Zhu, R. Yu, W. Zhang, E. Cui, X. Chen, Y. Dai, L. Cui, J. Li, L. Zhou, W. Chen, Z. Wang and L. Mai, Coordinating the edge defects of bismuth with sulfur for enhanced CO<sub>2</sub> electroreduction to formate, *Angew. Chem., Int. Ed.*, 2023, **62**, e202303117.
- 38 J. Wu, X. Yu, H. He, C. Yang, D. Xia, L. Wang, J. Huang, N. Zhao, F. Tang, L. Deng and Y.-N. Liu, Bismuth-nanosheet-based catalysts with a reconstituted Bi<sup>0</sup> atom for promoting the electrocatalytic reduction of CO<sub>2</sub> to formate, *Ind. Eng. Chem. Res.*, 2022, **61**, 12383–12391.
- 39 H. Shen, Y. Zhao, L. Zhang, Y. He, S. Yang, T. Wang, Y. Cao, Y. Guo, Q. Zhang and H. Zhang, In-situ structuring of copper-doped bismuth catalyst for highly efficient CO<sub>2</sub> electrolysis to formate in ampere-level, *Adv. Energy Mater.*, 2023, **13**, 2202818.
- 40 P. Liu, H. Liu, S. Zhang, J. Wang and C. Wang, A general strategy for obtaining BiOX nanoplates derived Bi nanosheets as efficient CO<sub>2</sub> reduction catalysts by enhancing CO<sub>2</sub>•<sup>-</sup> adsorption and electron transfer, *J. Colloid Interface Sci.*, 2021, **602**, 740–747.
- 41 T. Wissink, A. J. W. Man, W. Chen, J. M. J. J. Heinrichs, R. C. J. van de Poll, M. C. Figueiredo and E. J. M. Hensen, Evolution of bismuth oxide catalysts during electrochemical CO<sub>2</sub> reduction, *J. CO<sub>2</sub> Util.*, 2023, **77**, 102604.
- 42 Y. Hu, D. Lu, W. Zhou, X. Wang and Y. Li, In situ construction of 3D low-coordinated bismuth nanosheets@Cu nanowire core-shell nanoarchitectures for superior CO<sub>2</sub> electroreduction activity, *J. Mater. Chem. A*, 2023, **11**, 1937–1943.
- 43 H. Zheng, G. Wu, G. Gao and X. Wang, The bismuth architecture assembled by nanotubes used as highly efficient electrocatalyst for CO<sub>2</sub> reduction to formate, *Chem. Eng. J.*, 2021, **421**, 129606.
- 44 D. Yao, C. Tang, A. Vasileff, X. Zhi, Y. Jiao and S.-Z. Qiao, The controllable reconstruction of Bi-MOFs for electrochemical CO<sub>2</sub> reduction through electrolyte and potential mediation, *Angew. Chem., Int. Ed.*, 2021, **60**, 18178–18184.
- 45 B. Ávila-Bolívar, M. Lopez Luna, F. Yang, A. Yoon, V. Montiel, J. Solla-Gullón, S. W. Chee and B. Roldan Cuenya, Revealing the intrinsic restructuring of Bi<sub>2</sub>O<sub>3</sub> nanoparticles into Bi nanosheets during electrochemical CO<sub>2</sub> reduction, *ACS Appl. Mater. Interfaces*, 2024, **16**, 11552–11560.
- 46 Y. Wang, L. Cheng, J. Liu, C. Xiao, B. Zhang, Q. Xiong, T. Zhang, Z. Jiang, H. Jiang, Y. Zhu, Y. Li and C. Li, Rich bismuth-oxygen bonds in bismuth derivatives from Bi<sub>2</sub>S<sub>3</sub> pre-catalysts promote the electrochemical reduction of CO<sub>2</sub>, *ChemElectroChem*, 2020, **7**, 2864–2868.
- 47 D. Wang, K. Chang, Y. Zhang, Y. Wang, Q. Liu, Z. Wang, D. Ding, Y. Cui, C. Pan, Y. Lou, Y. Zhu and Y. Zhang, Unravelling the electrocatalytic activity of bismuth nanosheets towards carbon dioxide reduction: Edge plane versus basal plane, *Appl. Catal., B*, 2021, **299**, 120693.
- 48 Y. Jiang, Q. Chen, D. Wang, X. Li, Y. Xu, Z. Xu and G. Guo, In situ structural evolution of BiOCOOH nanowires and their performance towards electrocatalytic CO<sub>2</sub> reduction, *Nano Res.*, 2023, **16**, 6661–6669.
- 49 X. Zeng, C. Xiao, L. Liao, Z. Tu, Z. Lai, K. Xiong and Y. Wen, Two-dimensional (2D) TM-tetrahydroxyquinone metal-organic framework for selective CO<sub>2</sub> electrocatalysis: A DFT investigation, *Nanomaterials*, 2022, **12**, 4049.
- 50 Q. Liu, X. Bai, H. Pham, J. Hu and C. Z. Dinu, Active nanointerfaces based on enzyme carbonic anhydrase and metal-organic framework for carbon dioxide reduction, *Nanomaterials*, 2021, **11**, 1008.
- 51 F. Li, G. H. Gu, C. Choi, P. Kolla, S. Hong, T.-S. Wu, Y.-L. Soo, J. Masa, S. Mukerjee, Y. Jung, J. Qiu and Z. Sun, Highly stable two-dimensional bismuth metal-organic frameworks for efficient electrochemical reduction of CO<sub>2</sub>, *Appl. Catal., B*, 2020, **277**, 119241.
- 52 J. Wang, G. Chao, W. Zong, K. Chu, J. Zhu, R. Chen, Y. Zheng, L. Zhang and T. Liu, Efficient nitrate electroreduction to ammonia over copper catalysts supported on electron-delocalized covalent organic frameworks, *Chem. Eng. J.*, 2024, **499**, 156343.
- 53 P. Lamagni, M. Miola, J. Catalano, M. S. Hvid, M. A. H. Mamakhel, M. Christensen, M. R. Madsen, H. S. Jeppesen, X.-M. Hu, K. Daasbjerg, T. Skrydstrup and N. Lock, Restructuring metal-organic frameworks to nanoscale bismuth electrocatalysts for highly active and selective CO<sub>2</sub> reduction to formate, *Adv. Funct. Mater.*, 2020, **30**, 1910408.
- 54 L. Liu, K. Yao, J. Fu, Y. Huang, N. Li and H. Liang, Bismuth metal-organic framework for electroreduction of carbon dioxide, *Colloids Surf., A*, 2022, **633**, 127840.
- 55 W.-J. Xie, O. M. Mulina, A. O. Terent'ev and L.-N. He, Metal-organic frameworks for electrocatalytic CO<sub>2</sub> reduction into formic acid, *Catalysts*, 2023, **13**, 1109.
- 56 L. Cao, J. Huang, X. Wu, B. Ma, Q. Xu, Y. Zhong, Y. Wu, M. Sun and L. Yu, Active-site stabilized Bi metal-organic framework-based catalyst for highly active and selective electroreduction of CO<sub>2</sub> to formate over a wide potential window, *Nanoscale*, 2023, **15**, 19522–19532.
- 57 Q. Huang, X. Sha, R. Yang, H. Li and J. Peng, Electrochemical conversion of CO<sub>2</sub> into formate boosted by in situ reconstruction of Bi-MOF to Bi<sub>2</sub>O<sub>2</sub>CO<sub>3</sub> ultrathin nanosheets, *ACS Appl. Mater. Interfaces*, 2024, **16**, 13882–13892.
- 58 F. Yang, A. O. Elnabawy, R. Schimmenti, P. Song, J. Wang, Z. Peng, S. Yao, R. Deng, S. Song, Y. Lin, M. Mavrikakis and



- W. Xu, Bismuthene for highly efficient carbon dioxide electroreduction reaction, *Nat. Commun.*, 2020, **11**, 1088.
- 59 Z.-L. Yu, S.-Q. Wu, L.-W. Chen, Y.-C. Hao, X. Su, Z. Zhu, W.-Y. Gao, B. Wang and A.-X. Yin, Promoting the electrocatalytic reduction of CO<sub>2</sub> on ultrathin porous bismuth nanosheets with tunable surface-active sites and local pH environments, *ACS Appl. Mater. Interfaces*, 2022, **14**, 10648–10655.
- 60 R. G. Mariano, K. McKelvey, H. S. White and M. W. Kanan, Selective increase in CO<sub>2</sub> electroreduction activity at grain-boundary surface terminations, *Science*, 2017, **358**, 1187–1192.
- 61 Y.-M. Bai, C.-Q. Cheng, Z.-Z. Shi, X.-Z. Hu, S.-W. Yan, Z.-Y. Zhang, J. Yang, G.-R. Shen, P.-F. Yin, C.-K. Dong, H. Liu and X.-W. Du, Clean synthesis of bismuth porous nanosheets for efficient CO<sub>2</sub> electroreduction, *ACS Appl. Energy Mater.*, 2022, **5**, 11561–11567.
- 62 Y. Li, J. Chen, S. Chen, X. Liao, T. Zhao, F. Cheng and H. Wang, In situ confined growth of bismuth nanoribbons with active and robust edge sites for boosted CO<sub>2</sub> electroreduction, *ACS Energy Lett.*, 2022, **7**, 1454–1461.
- 63 L. Lin, X. He, X.-G. Zhang, W. Ma, B. Zhang, D. Wei, S. Xie, Q. Zhang, X. Yi and Y. Wang, A nanocomposite of bismuth clusters and Bi<sub>2</sub>O<sub>2</sub>CO<sub>3</sub> sheets for highly efficient electrocatalytic reduction of CO<sub>2</sub> to formate, *Angew. Chem., Int. Ed.*, 2023, **62**, e202214959.
- 64 Y. Wang, Z. Huang, Y. Lei, J. Wu, Y. Bai, X. Zhao, M. Liu, L. Zhan, S. Tang, X. Zhang, F. Luo and X. Xiong, Bismuth with abundant defects for electrocatalytic CO<sub>2</sub> reduction and Zn–CO<sub>2</sub> batteries, *Chem. Commun.*, 2022, **58**, 3621–3624.
- 65 J. Ren, X. Long, X. Wang, Z. Lin, R. Cai, M. Ju, Y. Qiu and S. Yang, Defect-rich heterostructured Bi-Based catalysts for efficient CO<sub>2</sub> reduction reaction to formate in wide operable windows, *Energy Technol.*, 2022, **10**, 2200561.
- 66 M. Wang, S. Liu, B. Chen, M. Huang and C. Peng, Co-regulation of intermediate binding and water activation in sulfur-doped bismuth nanosheets for electrocatalytic CO<sub>2</sub> reduction to formate, *Chem. Eng. J.*, 2023, **451**, 139056.
- 67 X. Chen, H. Chen, W. Zhou, Q. Zhang, Z. Yang, Z. Li, F. Yang, D. Wang, J. Ye and L. Liu, Boron dopant induced electron-rich bismuth for electrochemical CO<sub>2</sub> reduction with high solar energy conversion efficiency, *Small*, 2021, **17**, 2101128.
- 68 Y. Zhang, S. Liu, N. Ji, L. Wei, Q. Liang, J. Li, Z. Tian, J. Su and Q. Chen, Modulation of the electronic structure of metallic bismuth catalysts by cerium doping to facilitate electrocatalytic CO<sub>2</sub> reduction to formate, *J. Mater. Chem. A*, 2024, **12**, 7528–7535.
- 69 A. Xu, X. Chen, D. Wei, B. Chu, M. Yu, X. Yin and J. Xu, Regulating the electronic structure of bismuth nanosheets by titanium doping to boost CO<sub>2</sub> electroreduction and Zn–CO<sub>2</sub> batteries, *Small*, 2023, **19**, 2302253.
- 70 Y. Wang, B. Wang, W. Jiang, Z. Liu, J. Zhang, L. Gao and W. Yao, Sub-2 nm ultra-thin Bi<sub>2</sub>O<sub>2</sub>CO<sub>3</sub> nanosheets with abundant Bi–O structures toward formic acid electroreduction over a wide potential window, *Nano Res.*, 2022, **15**, 2919–2927.
- 71 Y. Fu, K. Leng, H. Zhuo, W. Liu, L. Liu, G. Zhou and J. Tang, Nanoconfinement effects on CuBi<sub>3</sub> alloy catalyst for efficient CO<sub>2</sub> electroreduction to formic acid, *J. CO<sub>2</sub> Util.*, 2023, **70**, 102456.
- 72 Y. Xiong, B. Wei, M. Wu, B. Hu, F. Zhu, J. Hao and W. Shi, Rapid synthesis of amorphous bimetallic copper-bismuth electrocatalysts for efficient electrochemical CO<sub>2</sub> reduction to formate in a wide potential window, *J. CO<sub>2</sub> Util.*, 2021, **51**, 101621.
- 73 W. Lou, L. Peng, R. He, Y. Liu and J. Qiao, CuBi electrocatalysts modulated to grow on derived copper foam for efficient CO<sub>2</sub>-to-formate conversion, *J. Colloid Interface Sci.*, 2022, **606**, 994–1003.
- 74 M. Wang, S. Liu, B. Chen, F. Tian and C. Peng, Synergistic geometric and electronic effects in Bi–Cu bimetallic catalysts for CO<sub>2</sub> electroreduction to formate over a wide potential window, *ACS Sustainable Chem. Eng.*, 2022, **10**, 5693–5701.
- 75 M. Tian, S. Wu, Y. Hu, Z. Mu, Z. Li, Y. Hou, P. Xi and C.-H. Yan, Doping and pretreatment optimized the adsorption of \*OCHO on bismuth for the electrocatalytic reduction of CO<sub>2</sub> to formate, *Nanoscale*, 2023, **15**, 4477–4487.
- 76 X. Yang, Q. Wang, F. Chen, H. Zang, C. Liu, N. Yu and B. Geng, In-situ electrochemical restructuring of Cu<sub>2</sub>BiS<sub>x</sub> solid solution into Bi/Cu<sub>x</sub>S<sub>y</sub> heterointerfaces enabling stabilization intermediates for high-performance CO<sub>2</sub> electroreduction to formate, *Nano Res.*, 2023, **16**, 7974–7981.
- 77 X. Zhang, L. Peng, B. Xu, P. Liu, X. Jiao, H. Kang, Z. Song, X. Yan, Y. Mao and J. Qiao, Bi–Cu bimetallic electrocatalysts prepared using electrochemical deposition effluent for highly converting CO<sub>2</sub> to formate, *Process Saf. Environ. Prot.*, 2022, **158**, 560–566.
- 78 Y. Xue, C. Li, X. Zhou, Z. Kuang, W. Zhao, Q. Zhang and H. Chen, MOF-derived Cu/Bi Bi-metallic catalyst to enhance selectivity toward formate for CO<sub>2</sub> electroreduction, *ChemElectroChem*, 2022, **9**, e202101648.
- 79 B. Liu, Y. Xie, X. Wang, C. Gao, Z. Chen, J. Wu, H. Meng, Z. Song, S. Du and Z. Ren, Copper-triggered delocalization of bismuth p-orbital favours high-throughput CO<sub>2</sub> electroreduction, *Appl. Catal., B*, 2022, **301**, 120781.
- 80 S. Yang, H. Wang, Y. Xiong, M. Zhu, J. Sun, M. Jiang, P. Zhang, J. Wei, Y. Xing, Z. Tie and Z. Jin, Ultrafast Thermal shock synthesis and porosity engineering of 3D hierarchical Cu–Bi nanofoam electrodes for highly selective electrochemical CO<sub>2</sub> reduction, *Nano Lett.*, 2023, **23**, 10140–10147.
- 81 H. Li, X. Yue, J. Che, Z. Xiao, X. Yu, F. Sun, C. Xue and J. Xiang, High performance 3D self-supporting Cu–Bi aerogels for electrocatalytic reduction of CO<sub>2</sub> to formate, *ChemSusChem*, 2022, **15**, e202200226.
- 82 Z. Yang, H. Wang, X. Fei, W. Wang, Y. Zhao, X. Wang, X. Tan, Q. Zhao, H. Wang, J. Zhu, L. Zhou, H. Ning and M. Wu, MOF derived bimetallic CuBi catalysts with ultra-wide



- potential window for high-efficient electrochemical reduction of CO<sub>2</sub> to formate, *Appl. Catal., B*, 2021, **298**, 120571.
- 83 H. Ren, X. Wang, X. Zhou, T. Wang, Y. Liu, C. Wang, Q. Guan and W. Li, In-situ constructing Cu<sub>1</sub>Bi<sub>1</sub> bimetallic catalyst to promote the electroreduction of CO<sub>2</sub> to formate by synergistic electronic and geometric effects, *J. Energy Chem.*, 2023, **79**, 263–271.
- 84 S. Yang, Y. Sun, C. Wang, L. Lv, M. Hu, J. Jin and H. Xie, One-step co-electrodeposition of SnBi for efficient electrochemical reduction of carbon dioxide to formic acid, *Catal. Sci. Technol.*, 2023, **13**, 758–766.
- 85 X. Xu, Y. Wei, L. Mi, G. Pan, Y. He, S. Cai, C. Zheng, Y. Jiang, B. Chen, L. Li, S. Zhong, J. Huang, W. Hu and Y. Yu, Interstitial Sn-doping promotes electrocatalytic CO<sub>2</sub>-to-formate conversion on bismuth, *Sci. China Mater.*, 2023, **66**, 3539–3546.
- 86 N. Sabouhanian, J. Lipkowski and A. Chen, Growth and electrochemical study of bismuth nanodendrites as an efficient catalyst for CO<sub>2</sub> reduction, *ACS Appl. Mater. Interfaces*, 2024, **16**, 21895–21904.
- 87 J. Zhou, L. Li, H. Ren, H. Wang, Y. Li, K. Liu, L. Huang, X. Yang, Z. Hao, Y. Zhang, Z. Wang, X. Wang, J. Ding, Y. Ji, L. Wang and H. Liang, A defective bismuth–indium catalyst promotes water dissociation for selective carbon dioxide electroreduction to HCOOH, *Inorg. Chem. Front.*, 2024, **11**, 1703–1709.
- 88 R. Wang, S. Deng, Y. Pang and G. Chai, Designing Bi-In<sub>2</sub>O<sub>3</sub> nanoflower catalysts for enhanced performance of electrochemical CO<sub>2</sub> reduction to formate, *ChemNanoMat*, 2024, **10**, e202400008.
- 89 Z. Yang, H. Wang, X. Bi, X. Tan, Y. Zhao, W. Wang, Y. Zou, H. Wang, H. Ning and M. Wu, Bimetallic In<sub>2</sub>O<sub>3</sub>/Bi<sub>2</sub>O<sub>3</sub> catalysts enable highly selective CO<sub>2</sub> electroreduction to formate within ultra-broad potential windows, *Energy Environ. Mater.*, 2024, **7**, e12508.
- 90 Q. Wang, X. Yang, H. Zang, F. Chen, C. Wang, N. Yu and B. Geng, Metal–organic framework-derived BiIn bimetallic oxide nanoparticles embedded in carbon networks for efficient electrochemical reduction of CO<sub>2</sub> to formate, *Inorg. Chem.*, 2022, **61**, 12003–12011.
- 91 T. Zhang, Y. Qiu, P. Yao, X. Li and H. Zhang, Bi-modified Zn catalyst for efficient CO<sub>2</sub> electrochemical reduction to formate, *ACS Sustainable Chem. Eng.*, 2019, **7**, 15190–15196.
- 92 C. Azenha, C. Mateos-Pedrero, M. Alvarez-Guerra, A. Irabien and A. Mendes, Binary copper-bismuth catalysts for the electrochemical reduction of CO<sub>2</sub>: Study on surface properties and catalytic activity, *Chem. Eng. J.*, 2022, **445**, 136575.
- 93 Z. Wang, Q. Yuan, J. Shan, Z. Jiang, P. Xu, Y. Hu, J. Zhou, L. Wu, Z. Niu, J. Sun, T. Cheng and W. A. I. Goddard, Highly selective electrocatalytic reduction of CO<sub>2</sub> into methane on Cu–Bi nanoalloys, *J. Phys. Chem. Lett.*, 2020, **11**, 7261–7266.
- 94 Y. Cao, S. Chen, S. Bo, W. Fan, J. Li, C. Jia, Z. Zhou, Q. Liu, L. Zheng and F. Zhang, Single atom Bi decorated copper alloy enables C–C coupling for electrocatalytic reduction of CO<sub>2</sub> into C<sub>2+</sub> Products, *Angew. Chem., Int. Ed.*, 2023, **62**, e202303048.
- 95 X.-D. Liang, Q.-Z. Zheng, N. Wei, Y.-Y. Lou, S.-N. Hu, K.-M. Zhao, H.-G. Liao, N. Tian, Z.-Y. Zhou and S.-G. Sun, In-situ constructing Bi@Bi<sub>2</sub>O<sub>3</sub>CO<sub>3</sub> nanosheet catalyst for ampere-level CO<sub>2</sub> electroreduction to formate, *Nano Energy*, 2023, **114**, 108638.
- 96 P. Deng, H. Wang, R. Qi, J. Zhu, S. Chen, F. Yang, L. Zhou, K. Qi, H. Liu and B. Y. Xia, Bismuth oxides with enhanced bismuth–oxygen structure for efficient electrochemical reduction of carbon dioxide to formate, *ACS Catal.*, 2020, **10**, 743–750.
- 97 X. An, S. Li, X. Hao, X. Du, T. Yu, Z. Wang, X. Hao, A. Abudula and G. Guan, The in situ morphology transformation of bismuth-based catalysts for the effective electroreduction of carbon dioxide, *Sustainable Energy Fuels*, 2020, **4**, 2831–2840.
- 98 J. Zeng, N. B. D. Monti, T. Chen, M. Castellino, W. Ju, M. A. O. Lourenço, P. Jagdale and C. F. Pirri, Evolution of bismuth electrodes activating electrosynthesis of formate from carbon dioxide reduction, *Catal. Today*, 2024, **437**, 114743.
- 99 Y. Zhang, Y. Chen, R. Liu, X. Wang, H. Liu, Y. Zhu, Q. Qian, Y. Feng, M. Cheng and G. Zhang, Oxygen vacancy stabilized Bi<sub>2</sub>O<sub>3</sub>CO<sub>3</sub> nanosheet for CO<sub>2</sub> electroreduction at low overpotential enables energy efficient CO-production of formate, *InfoMat*, 2023, **5**, e12375.
- 100 S. Abner and A. Chen, Nanostructured cobalt/copper catalysts for efficient electrochemical carbon dioxide reduction, *Nanoscale*, 2024, **16**, 12967–12981.
- 101 C. Cao, D.-D. Ma, J.-F. Gu, X. Xie, G. Zeng, X. Li, S.-G. Han, Q.-L. Zhu, X.-T. Wu and Q. Xu, Metal–organic layers leading to atomically thin bismuthene for efficient carbon dioxide electroreduction to liquid fuel, *Angew. Chem., Int. Ed.*, 2020, **59**, 15014–15020.
- 102 M. Serafini, F. Mariani, F. Basile, E. Scavetta and D. Tonelli, From traditional to new benchmark catalysts for CO<sub>2</sub> electroreduction, *Nanomaterials*, 2023, **13**, 1723.
- 103 K. Wang, T. Qu, Q. Li, S. Tan and X. Chen, Techno-economic analysis of electrocatalytic CO<sub>2</sub> reduction into methanol: A comparative study between alkaline flow cell and neutral membrane electrode assembly, *Catalysts*, 2023, **13**, 1005.
- 104 Z. Mi, A. Arbor and W. Jae Dong, *US Pat.*, 20240301573A1, 2024.
- 105 R. Parajuli, D. Ansovini, M. Philips and K. Schouten, *World Intellectual Property Organization Pat.*, 2019141827A1, 2019.
- 106 W. Li, C. Yu, X. Tan, Y. Ren, Y. Zhang, S. Cui, Y. Yang and J. Qiu, Beyond leverage in activity and stability toward CO<sub>2</sub> electroreduction to formate over a bismuth catalyst, *ACS Catal.*, 2024, **14**, 8050–8061.
- 107 J. Zhu, J. Li, R. Lu, R. Yu, S. Zhao, C. Li, L. Lv, L. Xia, X. Chen, W. Cai, J. Meng, W. Zhang, X. Pan, X. Hong, Y. Dai, Y. Mao, J. Li, L. Zhou, G. He, Q. Pang, Y. Zhao, C. Xia, Z. Wang, L. Dai and L. Mai, Surface passivation for highly active, selective, stable, and scalable CO<sub>2</sub> electroreduction, *Nat. Commun.*, 2023, **14**, 4670.



- 108 P. An, L. Wei, H. Li, B. Yang, K. Liu, J. Fu, H. Li, H. Liu, J. Hu, Y.-R. Lu, H. Pan, T.-S. Chan, N. Zhang and M. Liu, Enhancing CO<sub>2</sub> reduction by suppressing hydrogen evolution with polytetrafluoroethylene protected copper nanoneedles, *J. Mater. Chem. A*, 2020, **8**, 15936–15941.
- 109 J. Guo, X. Zhi, D. Wang, L. Qu, A. Zavabeti, Q. Fan, Y. Zhang, J. D. Butson, J. Yang, C. Wu, J. Z. Liu, G. Hu, X. Fan and G. K. Li, Surface-enriched room-temperature liquid bismuth for catalytic CO<sub>2</sub> reduction, *Small*, 2024, **20**, 2401777.
- 110 C. Lin, Y. Liu, X. Kong, Z. Geng and J. Zeng, Electrodeposited highly-oriented bismuth microparticles for efficient CO<sub>2</sub> electroreduction into formate, *Nano Res.*, 2022, **15**, 10078–10083.
- 111 L. Peng, Y. Wang, Y. Wang, N. Xu, W. Lou, P. Liu, D. Cai, H. Huang and J. Qiao, Separated growth of Bi-Cu bimetallic electrocatalysts on defective copper foam for highly converting CO<sub>2</sub> to formate with alkaline anion-exchange membrane beyond KHCO<sub>3</sub> electrolyte, *Appl. Catal., B*, 2021, **288**, 120003.
- 112 T. Dong, H. Li, Z. Wang, Y. Geng, R. Chang, X. Tian, J. Lai, S. Feng and L. Wang, Acidic electroreduction CO<sub>2</sub> to formic acid via interfacial modification of Bi nanoparticles at industrial-level current, *Nano Res.*, 2023, **17**, 5817–5825.
- 113 Y. Qiao, W. Lai, K. Huang, T. Yu, Q. Wang, L. Gao, Z. Yang, Z. Ma, T. Sun, M. Liu, C. Lian and H. Huang, Engineering the local microenvironment over Bi nanosheets for highly selective electrocatalytic conversion of CO<sub>2</sub> to HCOOH in strong acid, *ACS Catal.*, 2022, **12**, 2357–2364.
- 114 C. Qin, L. Xu, J. Zhang, J. Wang, J. He, D. Liu, J. Yang, J.-D. Xiao, X. Chen, H.-B. Li, Z. Yang and J. Wang, Phase interface regulating on amorphous/crystalline bismuth catalyst for boosted electrocatalytic CO<sub>2</sub> reduction to formate, *ACS Appl. Mater. Interfaces*, 2023, **15**, 47016–47024.
- 115 S.-F. Tang, X.-L. Lu, C. Zhang, Z.-W. Wei, R. Si and T.-B. Lu, Decorating graphdiyne on ultrathin bismuth subcarbonate nanosheets to promote CO<sub>2</sub> electroreduction to formate, *Sci. Bull.*, 2021, **66**, 1533–1541.
- 116 T. Fan, W. Ma, M. Xie, H. Liu, J. Zhang, S. Yang, P. Huang, Y. Dong, Z. Chen and X. Yi, Achieving high current density for electrocatalytic reduction of CO<sub>2</sub> to formate on bismuth-based catalysts, *Cell Rep. Phys. Sci.*, 2021, **2**, 100353.
- 117 F. Yang, Z. Xie, X. Huang, X. Yin, W. Zhang, Y. Huang and D. Zhang, Bi<sub>2</sub>S<sub>3</sub> nanorods grown on multiwalled carbon nanotubes as highly active catalysts for CO<sub>2</sub> electroreduction to formate, *Phys. Chem. Chem. Phys.*, 2023, **25**, 9198–9207.
- 118 L. Li, X. Jin, X. Yu and M. Zhong, Bimetallic Cu-Bi catalysts for efficient electroreduction of CO<sub>2</sub> to formate, *Front. Chem.*, 2022, **10**, 983778.
- 119 Y. Zhang, C. Cao, X.-T. Wu and Q.-L. Zhu, Three-dimensional porous copper-decorated bismuth-based nanofoam for boosting the electrochemical reduction of CO<sub>2</sub> to formate, *Inorg. Chem. Front.*, 2021, **8**, 2461–2467.
- 120 H. Jiang, L. Wang, Y. Li, B. Gao, Y. Guo, C. Yan, M. Zhuo, H. Wang and S. Zhao, High-selectivity electrochemical CO<sub>2</sub> reduction to formate at low overpotential over Bi catalyst with hexagonal sheet structure, *Appl. Surf. Sci.*, 2021, **541**, 148577.
- 121 X. Li, X. Wu, J. Li, J. Huang, L. Ji, Z. Leng, N. Qian, D. Yang and H. Zhang, Sn-Doped Bi<sub>2</sub>O<sub>3</sub> nanosheets for highly efficient electrochemical CO<sub>2</sub> reduction toward formate production, *Nanoscale*, 2021, **13**, 19610–19616.
- 122 B. Ren, G. Wen, R. Gao, D. Luo, Z. Zhang, W. Qiu, Q. Ma, X. Wang, Y. Cui, L. Ricardez-Sandoval, A. Yu and Z. Chen, Nano-crumpled induced Sn-Bi bimetallic interface pattern with moderate electron bank for highly efficient CO<sub>2</sub> electroreduction, *Nat. Commun.*, 2022, **13**, 2486.
- 123 Q. Yang, Q. Wu, Y. Liu, S. Luo, X. Wu, X. Zhao, H. Zou, B. Long, W. Chen, Y. Liao, L. Li, P. K. Shen, L. Duan and Z. Quan, Novel Bi-doped amorphous SnO<sub>x</sub> nanoshells for efficient electrochemical CO<sub>2</sub> reduction into formate at low overpotentials, *Adv. Mater.*, 2020, **32**, 2002822.
- 124 Y. Guan, X. Zhang, Y. Zhang, T. N. V. Karsili, M. Fan, Y. Liu, B. Marchetti and X.-D. Zhou, Achieving high selectivity towards electro-conversion of CO<sub>2</sub> using In-doped Bi derived from metal-organic frameworks, *J. Colloid Interface Sci.*, 2022, **612**, 235–245.
- 125 S. Li, Y. Kang, C. Mo, Y. Peng, H. Ma and J. Peng, Nitrogen-doped bismuth nanosheet as an efficient electrocatalyst to CO<sub>2</sub> reduction for production of formate, *Int. J. Mol. Sci.*, 2022, **23**, 14485.
- 126 F. Zhang, C. Chen, S. Yan, J. Zhong, B. Zhang and Z. Cheng, Cu@Bi nanocone induced efficient reduction of CO<sub>2</sub> to formate with high current density, *Appl. Catal., A*, 2020, **598**, 117545.
- 127 Z. Wu, H. Wu, W. Cai, Z. Wen, B. Jia, L. Wang, W. Jin and T. Ma, Engineering bismuth-tin interface in bimetallic aerogel with a 3D porous structure for highly selective electrocatalytic CO<sub>2</sub> reduction to HCOOH, *Angew. Chem., Int. Ed.*, 2021, **60**, 12554–12559.

